Chapter 14
Probing Molecular Photoexcited Dynamics by Soft X-Rays

Markus Gühr

Abstract This chapter presents a short introduction into probing photoexcited dynamics of isolated molecules by ultrashort x-ray pulses. It describes the basic concepts of electronic and nuclear dynamics in a molecule after optical excitation and shows basic concepts like element and site specific probing associated with x-rays. It discusses ultrafast x-ray sources for molecular spectroscopy and presents some of the very first gas phase molecular dynamics results that this young field has produced.

14.1 Introduction

We are currently in the second decade of ultrafast x-rays. Since 2000, ultrafast x-ray sources have been operating at synchrotrons [1]. With the first light from the free electron laser in Hamburg/Germany (FLASH) [2], the Linac coherent light source in SLAC National Accelerator lab [3], and SACLA in Japan [4] the brilliance of ultrafast extreme ultraviolet and x-ray sources has been increased by several orders of magnitude [5]. This chapter outlines the new possibilities using the brilliant and short soft x-ray pulses for probing the photodynamics of isolated molecules in the gas phase. While many interesting applications are found in solution phase, the photoexcited dynamics of isolated molecules offer a great chance for fundamental understanding [6, 7] since the highest accuracy simulations can be performed for these systems.

The key question in the molecule-light interaction is about the conversion of light energy into other forms of energy. The light does not provide any information on how its energy needs to get converted; different molecules however show very different conversion pathways after excitation. While some transform a large fraction of the

M. Gühr (✉)
PULSE, SLAC National Accelerator Laboratory and Stanford University,
2575 Sand Hill Road, Menlo Park, CA 94025, USA
e-mail: mguehr@stanford.edu

light energy into making different bonds resulting in a molecular geometry change, others distribute the photon energy over many vibrational modes leading to heating without bond change.

A few examples show the diversity of the molecular energy conversion after interaction with light. Many molecules undergo a major structural change localized around few bonds under light illumination [8]. Prominent examples are azobenzene [9, 10], stilbene [11, 12], rhodopsin, which is important for vision [13, 14] and in bacterial light harvesting [15, 16], and green fluorescent protein (GFP), used as fluorescent marker in genetics [17]. A prominent class of molecules that does not show any major structural change after photoexcitation is the nucleobases. Here, light energy is not directed towards the large amplitude motion of one particular molecular coordinate, but many molecular modes are "heated". It is argued, that the light-to-heat-conversion in nucleobases contributes to the photoprotection of our genetic code, by avoiding ultraviolet induced dimerization of neighboring bases in the DNA strand [18–20].

How does this efficient and selective usage of light energy emerge? The optical light is absorbed by valence electrons which are delocalized and mediate chemical binding. Upon light absorption, the valence electrons change their shape and a concerted motion of electrons and nuclei follows. In this complex dynamics on the photoexcited state, some channels for energy conversion are preferred over others and the fastest (accessible) process dominates the energy conversion [21–25]. Dictated by the Einstein rate coefficients, radiative processes on photoexcited states typically happen on the nanosecond time scale for ultraviolet to visible light. Much faster and thus more efficient reaction channels are provided by radiationless processes resulting from the coupling of nuclear and electronic motion in the photoexcited state. Typical timescales for these processes lie in the ultrafast domain of pico- to femtoseconds, requiring ultrafast tools for their observation.

The rest of this chapter will give and account on the use of ultrafast x-ray probes to for photoexcited dynamics. The topic is approached for isolated molecules, having the above mentioned advantage of very high level simulation capabilities. Moreover, gas phase spectroscopy allows a wide variety of probe methods. Besides time and energy resolved ion or electron spectroscopic methods, also coincidence methods for charged particles (ions and electrons) can be used giving very detailed information on the molecular state at the time of the probe interaction [26]. While demonstrating the main statements in this chapter on a general level, more detail will be presented for the case of nucleobases. These molecules have been studied by ultrafast optical methods for a long time and a rich experimental and theoretical literature is evidence of the interesting processes occurring in their photoexcited states. The nucleobases have also been studied thoroughly with many x-ray methods and in addition a time resolved study on the photoexcited dynamics has been performed recently with ultrafast soft x-rays at the LCLS [27].

The following section will describe some basics of potential energy surfaces (PESs) and nonradiative processes that cannot be described using the Born-Oppenheimer approximation (BOA) [28]. It is believed, that most optically excited

polyatomic molecules posses geometries at which nonradiative processes become determining in the energy conversion process [25, 29].

The third section of this chapter will introduce the concept of element and site selective probing and chemical shifts observed in x-ray spectroscopy [30–33], which can be used to address particular sites within the molecule. In the fourth section, crucial parameters of ultrafast x-ray sources will be presented and their usability for different x-ray spectroscopic methods discussed. The final section discusses the first examples of ultrafast x-ray probe experiments on photoexcited molecular states with an emphasis on the ultrafast x-ray Auger probing of nucleobase dynamics.

Ultrafast x-rays provide an important extension in the ultrafast toolbox due to their element and site selective probe character. The core wave functions involved in the x-ray probe transitions are extremely tightly bound which results in a high the local sensitivity within a molecule [34]. While the purpose of this chapter is to show how useful these new ultrafast x-ray probes can be and what promise they show for the future, it is mandatory to say that the new methods stand on the shoulders of giants. Ultrafast optical probe studies of light induced dynamics have been extremely successful and it is impossible in this context to give an overview of the most important works contributing to our understanding of photoexcited dynamics. I would understand the new ultrafast x-ray probe methods in this context: they are a valuable extension and maybe a crucial tool for many processes. Their real value however will lie in the complementarity to the optical ultrafast methods.

14.2 Molecular Processes

The interaction of optical light with molecules and the following molecular dynamics is the topic of many excellent textbooks [35–38]. In the following, the light induced dynamics is described, first using simple orbital arguments followed by a discussion of adiabatic potential energy surfaces. We then turn to vibrational relaxation and dynamics that cannot be described in the framework of the Born-Oppenheimer approximation.

In the beginning of any optically excited molecular dynamics is the interaction of valence electrons with light. The valence electrons are delocalized, that means they keep the molecule together by screening the repulsive forces between the positively charged nuclei, which are only in part screened by the core electrons. The absorption process results in a valence electron structure which is different from the "equilibrated" electronic ground state. This in turn will change the forces between the nuclei, resulting in nuclear dynamics. For the simple case of diatomic molecules, the light induced changes in the nuclear structure can be read from the change in equilibrium internuclear distance from ground to excited state. For Br_2, the ground state $^1\Sigma_g$ has a $R_e = 2.28$ Å. The optical excitation promotes one electron from a π_u orbital with no node orthogonal to molecular axis to a σ_u orbital with nodes [39, 40]. The reduced electron density in between the nuclei results in an expanded excited state ($^3\Pi_u$) with $R_e = 2.66$ Å
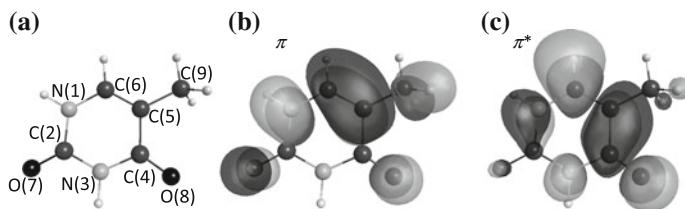
Fig. 14.1 Nuclear structure (**a**), second highest occupied molecular orbital (HOMO-1) π and lowest unoccupied molecular orbital (LUMO) π* in (**b**) and (**c**) respectively. Ultraviolet radiation induces the so called ππ* transition, in which one electron is promoted from the π into the π* orbital. Due to the nodal structure of the orbitals, one expects an elongation of the C(5)–C(6) and C(4)–O(8) bond as well as a contraction of the C(4)–C(5) bond after photoexcitation

For the case of thymine, the excitation scheme is displayed in Fig. 14.1. The light accomplishes a so called π−π* excitation, promoting and electron from a π orbital as shown in Fig. 14.1b into the π* orbital in Fig. 14.1c. The π orbital shows high electron density in between atoms C(5)–C(6), and a node in the C(4) atom. The newly populated π* orbital shows a node in between C(5)–C(6) as well as in between C(4)–O(8) leading to reduced electron density triggering bond elongation. On the C(4)–C(5) bond, the π* orbital increases the electron density leading to a bond contraction in the excited state. These coordinates are said to be Frank-Condon active, since they are directly coupled to the electronic change upon light excitation. Calculation on a higher level confirm this simple picture [41, 42].

The light induced nuclear motion is described in terms of potential energy surfaces (PES) which are intimately connected to the Born-Oppenheimer approximation simplifying the molecular Schrödinger equation. First, the eigenvalues of the electronic part of the Hamiltonian are calculated for fixed nuclei. This can be done because the light electrons can adapt instantaneously to any change in the slow motion of the heavy nuclei. The electronic spectrum is repetitively calculated for many nuclear geometries; connecting them leads to adiabatic PES. Based on these potentials, the complete Hamiltonian is solved. During this step, the Born-Oppenheimer approximation [28] neglects coupling terms among different electronic states based on the fact that they scale with the ratio of electronic over nuclear mass.

In order to simulate the nuclear dynamics following optical excitation, a nuclear wavepacket is constructed by calculating the dipole matrix element of the ground state with the excited PES. Once more, the electronic and nuclear wavefunction are separated giving rise to an electronic transition dipole and a Franck-Condon matrix element between the vibrational eigenstates of the electronic ground state and those of the electronically excited state. For harmonic oscillator PES, the nuclear wavepacket undergoes repetitive motion, with periodic recurrence in position and shape. An harmonic oscillator in one nuclear dimension leads to wavepacket dephasing followed by revivals of the wavepacket or of multiple copies at different positions [43–45]. For molecules with more than two nuclei an additional phenomenon called intermolecular vibrational redistribution (IVR) occurs. The initially excited Franck-Condon

active vibrational modes are anharmonically coupled to other vibrational modes. An excellent introduction to IVR has been presented by Nesbitt and Field [46].

The Born-Oppenheimer approximation is often not sufficient to describe photoexcited molecular dynamics. As two PES come close, the separation of electron and nuclear motion breaks down, which can be understood using an intuitive approach by Herzberg [47]. The key argument allowing for separation of electronic and nuclear degrees of freedom is that light and therefore fast electrons are adapting instantaneously to any changing geometry of the heavy and slow nuclei. In the quantum world, the timescale of motion for any quantum object is given by the inverse of the energy spacing $(1/\Delta E)$ of the eigenstates. Imagine just two electronic states being involved. Their ΔE changes as a function nuclear geometry. In the most extreme case, the nuclei can drive the quantum system to geometries where ΔE becomes very small or even zero. The electrons move slowly at these nuclear geometries and thus the electron-nuclear separation is not justified any more. A more formal derivation for example in [22, 28, 48] shows that the so called non-BOA coupling elements, which are based on the nuclear momentum operator, couple different adiabatic electronic states. The non-BOA couplings scale by the inverse energy spacing of PESs, which means that close lying adiabatic states are strongly coupled and wavepacket population is nonradiatively transferred from one adiabatic state to another. The nonradiative non-BOA transitions are fast, which means they are very efficient in driving excited state populations into particular channels.

A special class of topological constructs in which two adiabatic surfaces are close and even degenerate are the so called conical intersections (CIs). The PESs describe the shape of a cone around a point of degeneracy between the adiabatic states, leading to the nomenclature. The CIs were first proposed by Teller in 1937 [49] and afterwards mostly ignored as a kind of exotic topology. In the recent two decades however, conical intersections are intensely studied for their role in photoexcited dynamics [25, 29, 48, 50]. The dimensionality of a conical intersection is explained by Atchity et al. [51]: In an M dimensional nuclear geometry space, two particular geometry vectors g and h [50] span the CI and the point of degeneracy is a M-2 dimensional subspace, with certain exceptions based on symmetry arguments. Thus, in most molecules a "seam of conical intersections" [52] is lined up the nuclear geometry space.

Conical intersections are relevant for the photoexcited dynamics of thymine, the main example pursued in this contribution. Figure 14.2 presents a sketch of the ultraviolet excitation that initially populates the $\pi\pi^*$ state. Population is funneled into the lower lying $n\pi^*$ and ground state through conical intersections as the nuclear wave packet propagates. Directly after the photoexcitation, the planar relaxation coordinates described in the context of in Fig. 14.1 drive the wavepacket out of the Franck-Condon range. A ring folding coordinate gets activated which promotes the molecular wavepacket close to the conical intersections. Several intersections are predicted among the different states. The lowest energy intersections predicted by Hudock et al. [41] and Szymcak et al. [42] are sketched in Fig. 14.2. The g and h vectors for the intersection with $n\pi^*$ from [42] are shown in Fig. 14.2b; they illustrate the complexity of these coordinates. While g has a dominant contribution from
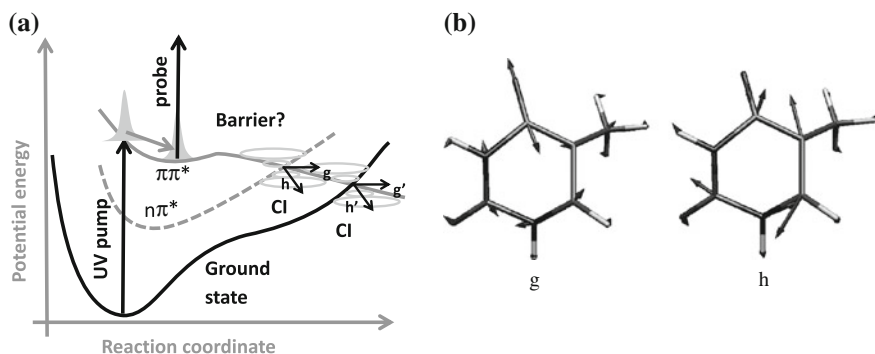
Fig. 14.2 a Reaction path from the Franck-Condon region to conical intersections with the ground and nπ* states. A barrier along the relaxation coordinate is object of discussion in the literature. **b** g and h vectors sketched by motion direction of certain atoms within the thymine molecule (reprinted with permission from [42]. Copyright 2009 American Chemical Society). These two vectors span the space for the conical intersection π π*-nπ*

the Franck-Condon active C–O stretch, the h vector possesses a strong out of plane component. The path from the Franck-Condon (FC) region to the conical intersections sketched here proceeds via an elongation of the C(5)–C(6) and C(4)–O(8) bond. A barrier in between the FC region and the CIs is indicated in Fig. 14.2. This barrier is currently matter of a debate and it is crucial for the molecular dynamics. Hudock et al. [41] and Szymcak et al. [42] predict a barrier that slows down electronic relaxation on the π π* state by trapping population in a minimum. According to these simulations, the molecular population in the π π* state needs several picoseconds to arrive at the CIs sketched in Fig. 14.2. Other groups use similar methods but slightly different basis sets and arrive at fundamentally different conclusions. Merchan et al. [53], Perun et al. [54] as well as Asturiol et al. [55] argue that the relaxation out of the π π* state occurs without any trapping of population behind a barrier, and thus electronic relaxation is expected to happen on a ∼100 fs timescale.

14.2.1 Experimental Work on Molecular Dynamics Outside the BOA Framework

Almost all ultrafast photoexcited dynamics measurements on molecules are done with light in the visible and ultraviolet domain. For the pump pulse, it is necessary to use this wavelength range if one wants to draw connections to molecular excitation by sunlight. Since the pump-pulse is optical, it is relatively practical to also use optical light for probing (sometimes the same color) which however is not necessary. In fact, the probe pulse is observing the phenomenon and its spectral range can be chosen according to whichever method is best suited.

In the gas phase most ultrafast experiments on neutral photoexcited molecules are performed by measuring ion yields or electron kinetic energy spectra as a function of pump-probe time delay, with additional parameters such as angular distribution. Multi-photon probing combined with ion counting have been among the first ultrafast probes of photoexcited dynamics [56, 57] and the strong field tunneling picture allows certain conclusions about the shape of the ionized orbital [58, 59]. In the following we concentrate on time resolved photoelectron spectroscopy, for which an excellent introduction has been provided by Stolow and Neumark [60, 61]. Energy and time resolved photoelectron spectroscopy is often able to distinguish ultrafast vibrational and electronic dynamics, as shown by Stolow and coworkers [62, 63]. The analysis of those spectra is based on the notion that ionization of a photoexcited neutral state occurs most likely upon removal of one only electron. If several cationic states are energetically accessible by the probe pulse, photoelectrons will reflect predominantly a transition to the ionic state requiring only removal of one electron.

In order to separate electronic from nuclear relaxation it is however necessary that: (1) the change in photoelectron energy due to competing vibrational relaxation does not infer with the change in photoelectron energy from the nonadiabatic transition and (2) the probe pulse needs to have a photon energy high enough to ionize the molecule despite vibrational and electronic relaxation [64]. As the molecular dynamics distributes energy into several nuclear degrees of freedom and at the same time also other electronic states, an optical photon is not energetic enough for many molecules to provide ionization. The general decay on the photoelectron signal is then not sufficient any more to distinguish vibrational and electronic relaxation. Barbatti and Ullrich recently elaborated on these aspects of optical time resolved photoelectron spectroscopy for the case of the nucleobase adenine [65].

For the example of the nucleobase thymine, past experiments are not interpreted in a coherent way, mostly due to the ambiguity between electronic and vibrational relaxation. Several experimental studies in liquids and isolated molecules confirm that the excited state dynamics occurs in the sub-picosecond and picosecond regime [19]. The isolated studies are best suited to be compared to the single molecule ab-initio theory discussed above. Time resolved ion yield experiments in the gas phase show a very short sub $100\,fs$ decay constant followed by additional $5\text{--}7\,ps$ decay [66–68]. The short decay has been interpreted by some authors as ultrafast electronic relaxation from the $\pi\pi^*$ state to the electronic ground state [67]. However, the fast initial dynamics can also be attributed to ultrafast nuclear relaxation as done in photoemission experiments [69]. The $500\,fs$ time constant found there was interpreted to display nuclear dynamics followed by population trapping in the $\pi\pi^*$ minimum [41]. As described above, the simulations are divided into two different classes: one set is predicting the ultrafast electronic relaxation into the electronic ground state on a few $100\,fs$ [53–55] not slowed down by a reaction barrier. The other class is predicting a reaction barrier, slowing down nonadiabatic electronic relaxation favoring the interpretation of fast decays as nuclear relaxation [41, 42]. Combining the experimental and theoretical studies in thymine, an 'ideal' experiment needs to be able to distinguish nuclear relaxation on the $\pi\pi^*$ state from electronic relaxation. In the latter case it should also be able to distinguish nonadiabatic transitions to the

nπ* state from those to the electronic ground state. Given the essential theoretical disagreement about the reaction barrier and the experimental dispute about analysis and interpretation of transients, it will be advantageous to measure the photoexcited dynamics with a drastically different method. We will describe such an attempt in the last section of this contribution. We choose ultrafast x-rays as probes of the molecular dynamics and we will therefore introduce basic concepts and advantages of molecular x-ray spectroscopy below.

14.3 Probing Molecular Electronic Structure by Soft X-Rays

Probing in the photoexcited states by ionization in the optical and vacuum ultraviolet range uses exclusively the mostly delocalized valence electrons. In the extreme ultraviolet (EUV, 30–280 eV) and soft and hard x-ray spectral domain however, light can couple to localized *core* electrons of distinct elements inside the molecule. Figure 14.3 shows the binding energies of important elements in the EUV and SXR region. As can be immediately seen, these energies are very distinct, which allows to individually address those elements by interaction with light. In the extreme ultraviolet, the M edges of the 3d transition metals provide element sensitivity. In the soft x-ray range, the K edges of oxygen, nitrogen and carbon as well as the L edges
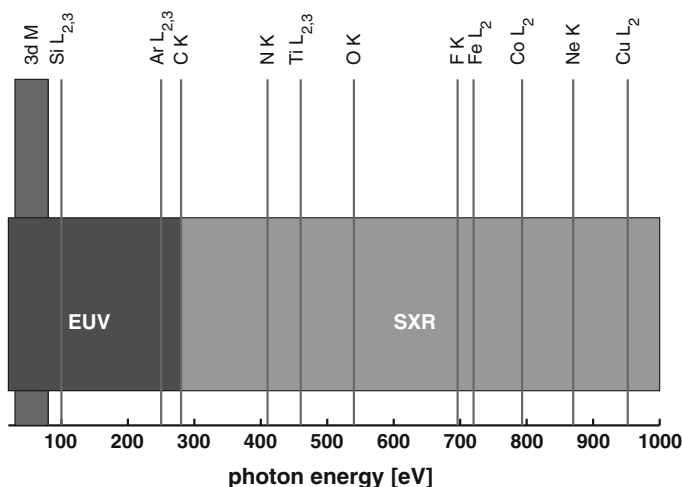

Fig. 14.3 Elemental edges in the extreme ultraviolet and soft x-ray spectral regions. The M edges of the 3d transition metals are due to 3p transitions, the K edges due to 1s absorption and the L edges due to 2s and 2p absorption.
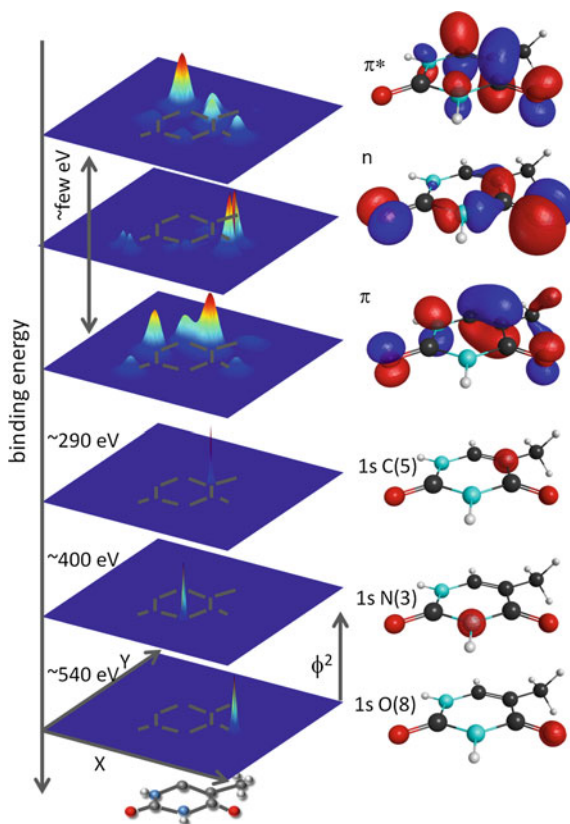
Fig. 14.4 Orbitals of the nucleobase thymine calculated using GAMESS and the 6–311 basis set. The *right hand column* shows isosurfaces of selected orbitals. On the upper part, three selected valence orbitals are shown. The π^* and π orbitals are mostly delocalized over the molecule whereas the lone pair n orbital consists of p like lobes at the two oxygen atoms. In the lower part of the picture, three representative 1s orbitals of carbon nitrogen and oxygen are shown with their binding energies. The core hole wavefunctions are extremely well localized at the respective atoms. The *left hand column* shows 2d representations of the orbitals. It is obtained by cutting through it in a plane parallel to the ring plane and taking the absolute

of 3d transition metals provide this element contrast due to the element specific energy of core levels. An overview of different core level binding energies is given in [30, 31, 70, 71].

The electronic wavefunctions of core electrons are extremely well localized in contrast to the valence wave functions that are in general delocalized over large parts of the molecule. Figure 14.4 shows two-dimensional cuts of some C, N, and O 1s orbitals of the thymine molecule together with some typical valence orbitals. The enormous difference in localization properties shows that any transition (or quantum mechanical matrix element) involving core electrons is necessarily very confined in
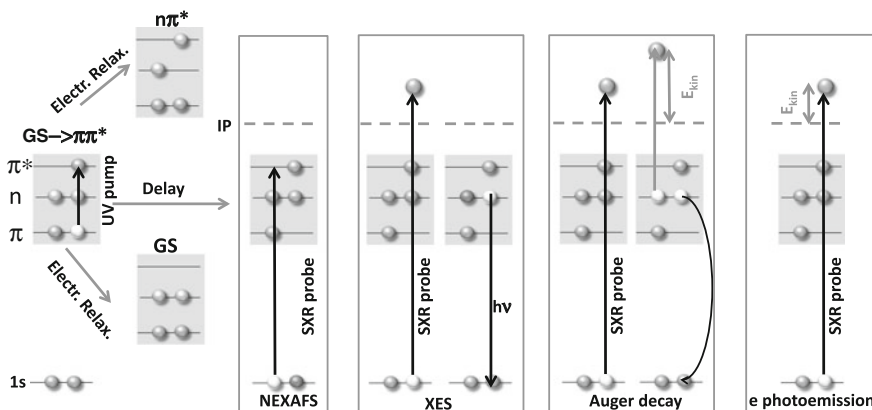
Fig. 14.5 Different schemes to probe transient electronic structure by x-ray interactions, exemplified on the important orbitals of thymine. The ultraviolet excitation pulse transfers population from the electronic ground state to the $\pi\pi*$ state. In near edge x-ray absorption fine structure (NEXAFS) spectroscopy, one probes the valence occupation by resonant absorption from the core levels. In x-ray emission spectroscopy, the core electron is promoted above the ionization limit and the emitted photons from valence electrons filling the core hole are spectrally resolved. In the soft x-ray region, photoemission is small; instead the Auger emission sketched in the third field is the prominent process. In this technique, the kinetic energy of the Auger electrons is analyzed. In x-ray photoelectron emission (XPS) one directly analyzes the kinetic energy of the emitted core electron

space. In the x-ray community this aspect is termed local sensitivity. Moreover, we will show below in the section on photoelectron spectroscopy that the core binding energies of an element depend on the nearest environment of binding partners. Although chemical shift is only fraction of an eV up to a few eV as compared to many 10 and 100 eV element shift, it is visible in spectra and can be used in time resolved studies. Generally the term site selectivity is reserved for this phenomenon. In the following we will discuss the element and site selectivity of x-ray absorption, x-ray photoemission, Auger electron emission and x-ray photoelectron spectroscopy. An excellent overview of different techniques for gas phase targets is given in [72, 73]. A graphical overview of the different techniques is shown in Fig. 14.5.

14.3.1 X-Ray Absorption

The progress in x-ray absorption spectroscopy until 1992 is documented in J. Stöhr's monograph [74]. The interpretation of near edge x-ray absorption fine structure (NEXAFS) spectra in the soft x-ray domain was systematically elaborated from small molecules [72, 73], to small molecules on surfaces [74, 75] and complex systems in solution [76, 77]. The interaction of light with a quantum system during absorption is described by the matrix element $\langle\phi_i|\mu|\phi_f\rangle$, where $\phi_{i,f}$ are the initial and final states

of the system and μ is the dipole operator. The initial state usually has completely filled shells up to the valence levels; the final state is described as a core hole and an additional electron in a valence or continuum state accompanied by some restructuring of valence electron due to electron correlation. The one electron approximation used from now on neglects the coupling among the electrons, which simplifies the description. Within the one electron approximation, the initial state of the absorption process can be represented by a core electron orbital. The final state in absorption spectroscopy is an *unoccupied* or *partially* occupied valence or a continuum orbital. Within the linear combination of atomic orbital (LCAO) approximation, the transition strength between core electron and unoccupied molecular valence states is then proportional to the atomic orbital coefficient at the core hole site of the respective molecular orbital [34, 74, 78]. Thus, one probes a highly local electronic property of valence electronic states. This picture can be helpful thinking about the applications of NEXAFS spectroscopy for photoexcited molecular dynamics. As pointed out in the previous section, the electronic character of photoexcited states undergoes transient changes. In the case of thymine, the π π* decays into an nπ* state upon electronic relaxation. Thereby the occupation changes from ($\pi^1 n^2 \pi^{*1}$) to ($\pi^2 n^1 \pi^{*1}$). Referring to Fig. 14.4, the transition between one of the oxygen 1 s electrons and the highly localized n orbital is must be very strong. The absorption 1s-n is not possible in the ground and π π* states since the n orbital is completely filled; it becomes allowed with the nonadiabatic transition to the nπ* state, offering a great chance for the direct detection of the non-BOA transition. It is worth mentioning that any molecule containing lone pair orbitals n among the highest occupied or lowest unoccupied orbitals provides highly localized valence orbitals. The processes involving the lone pair orbitals do not necessarily need to be restricted to the photorelaxation of a single molecule like in the nucleobase. For instance, the [2+2] photocycloaddition of carbonyl compounds, which is a bond formation, proceeds via an nπ* photoexcited state.

We demonstrate the content of NEXAFS spectra for thymine, discussing data from Plekan et al. [79] in Fig. 14.6. One identifies the sharp transitions to unoccupied molecular orbitals, which are of π* character. At the oxygen absorption edge, the two different oxygen sites O(7) and O(8) lead to a splitting of the lowest energy feature. The corresponding transitions involve two different π* orbitals, π_6^* corresponds to the orbital shown in Fig. 14.1c. As mentioned in the introduction to this section, we can clearly distinguish the O(7) and O(8) sites with ∼1 eV splitting. In contrast, the two lowest energy features in the nitrogen K absorption spectrum of thymine are not easily separated in terms of the two nitrogen atoms N(1) and N(3). The lines from 401 to 403 eV photon energy are mostly of mixed nature. At the carbon K edge however, the two lowest lines are due to a specific carbon atoms, the higher lying lines are of mixed character [79]. Towards higher energies, transitions between core electrons and molecular Rydberg states are excited and finally above the ionization limit an unstructured and very broad feature sets in. This feature is called multiple scattering or σ* resonance. It originates from the multiple electron scattering in the molecular potential made up by Coulomb forces and centrifugal barriers for states with high angular momentum [80–84].
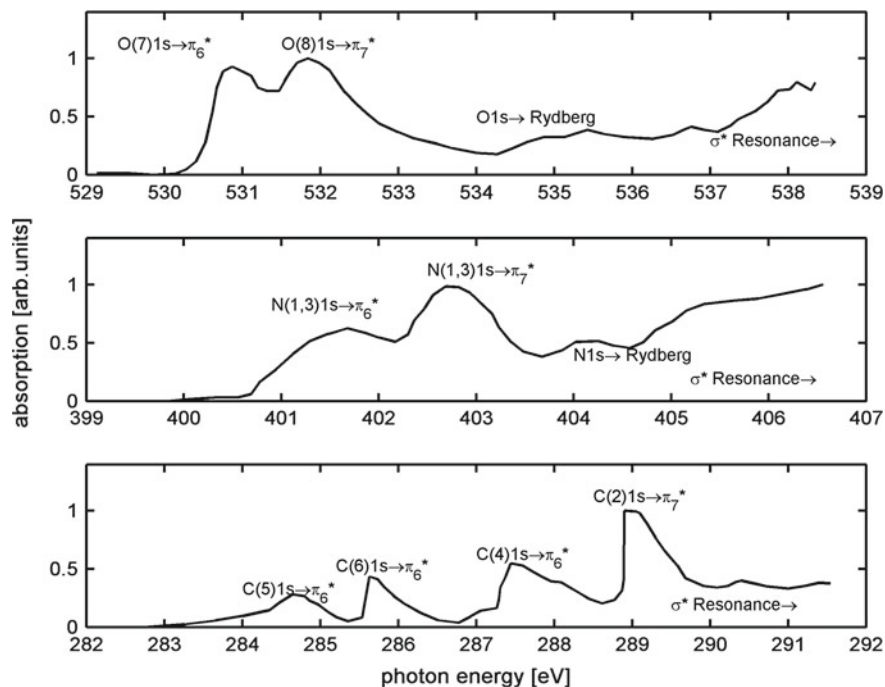
Fig. 14.6 Near edge x-ray absorption fine structure (NEXAFS) spectra of thymine at the oxygen (*top*), nitrogen (*middle*) and carbon (*bottom*) edges (reproduced by digitizing data from [79]). The labeled peaks correspond to transitions from ground state molecules to a state with a 1s core electron missing and an electron created in an initially unoccupied valence orbital. The orbital π_6^* corresponds to the orbital shown in Fig. 14.1c, π_7^* is not shown here but can be found in [79]. At the oxygen and carbon edges one identifies peaks that correspond to core hole creation at particular sites, for instance O(7) or O(8)

14.3.2 X-Ray Emission

X-ray (photo)emission spectroscopy (XES) can be described by the same matrix element as absorption; however the initial state is an *occupied* valence orbital the final state is a core orbital. Thus, XES possesses the same element and site selectivity as NEXAFS, with the big difference that XES monitors occupied orbitals, which makes the two methods ideally complementary. In the soft x-ray region, the decay of core ionized states via XES is in fierce competition with radiationless Auger decay. The time needed for an Auger decay into 1s states is typically in the domain of a few femtoseconds [85]. The photoemission time is governed by the Einstein rate coefficient for spontaneous decay, which is much slower than the Auger decay in the SXR range. Thus the relative yield of photoemission compared to Auger decay is low [85]. With increasing XES photon energy, the Einstein rate coefficient for spontaneous emission increases, leading to a much higher fluorescence yield in the

hard x-ray domain [86]. The low SXR yield, together with low apparatus efficiency due to limited angular acceptance of grazing incidence gratings [87], make XES applications for dilute systems very challenging. For small molecules, this problem can be easily be compensated using high pressures, as demonstrated for N_2 [88], O_2 [89], CO [90], and CO_2 [91]. Here, XES spectra are to first order attributed to certain molecular orbitals. For more complex molecules like transition metal complexes, multiplet effects need to be taken into account [92]. For nucleobases, the only XES spectra documented were obtained from solid samples at the nitrogen edge [93].

To use the soft x-ray emission technique for time resolved measurements on diluted isolated molecules, sources will have to provide much more average flux. Boosting single pulse energy will only lead to non-useful sequential molecular ionization. Instead, the repetition rate will have to be increased, which is exactly matched in the strategy for future FEL x-ray sources.

14.3.3 Auger Electron Emission and Fragmentation

The matrix element for Auger emission is much more complex compared to the dipole matrix element. The Auger decay of a core hole is described by a two electron operator $1/r_{12}$, whose eigenvalue reflects the inverse distance of two electrons. The Auger matrix element can be simplified to $\langle \phi_k \phi_l | 1/r_{12} | \phi_{core} \phi_{cont} \rangle$, where $\phi_k \phi_l$ are the two valence electron orbitals that fill the core hole and emit the Auger electron, ϕ_{core} is the initially ionized core orbital and ϕ_{cont} is the continuum orbital that is filled by the Auger electron [94, 95]. In summing over the different valence channels kl, the spin multiplicity needs to be taken into account properly [94]. If we neglect the electron interaction, the kinetic energy E_{kin} of an Auger electron is given as $E_{core} - E_k - E_l$, where $E_{core,k,l}$ are the binding energies of the core and two valence electrons. It is important to note here, that the photon energy does not influence the Auger kinetic energy, as long as complete core hole ionization into the continuum occurs. This makes this technique very attractive for FEL sources based on self amplified spontaneous emission (SASE). For those FELs, lasing starts from noise, which results in a large spectral shot-to-shot fluctuation [96].

The x-ray typical element selectivity and local sensitivity still holds, even for the more complex Auger decay. Since the core hole energy differs strongly depending on the element, the Auger decay energies from different elements within a molecule are separable (see Moddeman et al. [97] for element selected Auger spectra CO, NO, H_2O, and CO_2). The local sensitivity comes from the fact that the very narrow core orbital ϕ_{core} is included in the spatial integral of the matrix element. Early Auger spectroscopy on small di-and triatomic molecules [94, 98, 99] demonstrated that the Auger spectrum amplitude can be constructed reasonably enough by just tracking the atomic orbital coefficients at the core hole site of the LCAO constructed molecular orbitals $\phi_k \phi_l$. The molecular Auger spectra of 2p elements like carbon, nitrogen and oxygen separate into three different energy ranges. Figure 14.7 shows the oxygen

Fig. 14.7 Auger spectra of thymine in the electronic ground state. The *black* spectrum was measured at a synchrotron (advanced light source beamline 8), the *grey* spectrum at the free electron laser (Linac coherent light source)
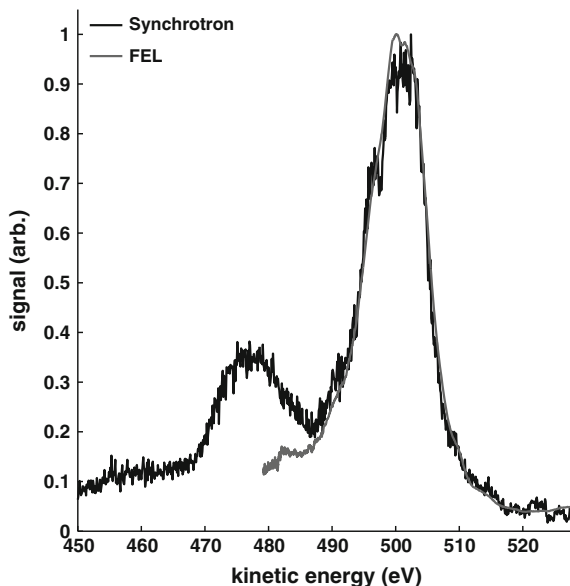
Auger spectrum of thymine. The highest kinetic energies around 500 eV result from Auger decay involving mostly two 2p valence orbitals, since those have the lowest binding energy. The group of Auger decay around 475 eV is due to valance orbitals of mixed character, one 2s and another 2p. The third and lowest kinetic energy group hardly visible from 450 to 460 eV is due to decays involving two 2s orbitals.

All of the Auger lines are lifetime broadened and identifying one particular channel or a particular decay site among equal elements is often impossible. Auger decay spectra measured and simulated by Storchi et al. on pyrimidine [100] (which is essentially the ring of without the methyl group and the oxygen atoms) exemplify this point. Figures 14.2 and 14.3 in [100] show Auger spectra due to nitrogen 1s core hole decay and carbon 1s core hole decay respectively. The kinetic energies of the different core hole Auger decays are very well separated by about 100 eV. The spectra consist of many lines, calculated here on the algebraic diagrammatic construction (ADC(2)) level [101, 102] and the isolation of one particular nitrogen or carbon core hole decay from the experimental spectrum is practically impossible.

The involvement of valence orbitals ϕ_k ϕ_l in the Auger decay makes Auger spectroscopy interesting for time resolved spectroscopy on photoexcited molecular states. Electronic relaxation changes the valence orbital occupation, SXR core hole ionization followed by Auger decay offers an observation opportunity for this process. Together with the element selectivity and local sensitivity, Auger decays at different core hole sites predominantly probe different orbitals. For the example of thymine in Fig. 14.4 it is obvious that the Auger decay of oxygen 1s vacancies predominantly probes the oxygen lone pair type orbitals. The C and N core hole decays do not

involve these lone pair but more likely to the π orbitals, which are delocalized over the ring. An important consideration for time resolved experiments is the fact that the Auger decay takes some time itself. For most practical experiments however, the few femtosecond time constant is short compared to the molecular dynamics.

The Auger decay into dicationic states with two valence electrons missing leads mostly to molecular fragmentation. This can be understood in an orbital picture in which initially binding orbitals become depleted by the Auger decay. Resonant excitation of small molecules into unoccupied molecular orbitals can lead to fragmentation at a particular site [103]. For thymine, fragmentation was induced by C ionization at different sites [104]. The larger molecules like thymine have a high density of dicationic states, all of which are occupied according to the Auger decay matrix element. This manifold of states mix strongly along the fragmentation path and it turns out that most fragment yields do *not* depend on the core hole site [104, 105]. Nevertheless, some thymine fragments show an interesting behavior on the core hole site. For instance, the creation of CO+ fragments is correlated to the core hole on C(2) and C(4), which are the C atoms connected to the two oxygen atoms in the molecule. For C(5) and C(6) core hole excitation, a strong site specific decay into $HNCOH^+$ and $C_4H_4ON^+$ was observed. Itälä et al. associate this decay to the participation of the π orbital (shown in Fig. 14.1b) in the Auger decay as the π orbital has a high amplitude at the C(5) and C(6) positions. The final states with π population missing after the Auger decay are very low in energy. Thus, they can only lead to fragmentation into the most stable fragments, which happen to be the $HNCOH^+$ and $C_4H_4ON^+$ fragments.

14.3.4 X-Ray Photoelectron Spectroscopy

X-ray photoelectron spectroscopy is one of the most advanced methods of all x-ray probes in the gas phase as well as in liquid or solid state [106]. Like in absorption spectroscopy described above, the dipole matrix element induces a transition, here between the core electron and a *continuum* state. The continuum electron possesses kinetic energy, leaving behind a molecule with a core hole. For different elements, core binding energies are very distinct. For one and the same element occurring on different sites within the molecule the photoelectron spectrum shows site splitting on the sub eV to eV scale as well as vibrational features on the meV scale. The binding energy depends on the environment of the core hole site. The valence electrons located close to the core site screen the nuclear potential leading to a lower binding energy. Reduced valence density results in less screening and higher binding energies. The resulting sensitivity on the chemical environment has been called chemical shift and gave rise to the ESCA (electron spectroscopy for chemical analysis) technique invented by Siegbahn [32]. A compilation of typical site specific molecular spectra can be found in the compilation by Jolly, Bomben, and Eyermann [107].

The local chemical environment depends on the exact nuclear geometry and the electronic structure that goes with it. Reduced concepts like electronegativity, partial atomic charge and polarizability are used to express the chemical sensitivity of core hole binding energies [108]. Site effects in the carbon photoelectron spectrum of thymine [79, 104, 109] again exemplify the electronegativity arguments. The electronegativity of atoms is increasing from carbon over nitrogen to oxygen. The C(2) atom, surrounded by two N and one O atoms, shows the lowest kinetic energy of all [79, 109] (note: [109] uses the standard nomenclature as in Fig. 14.1a whereas [79] uses a different one). Atom C(4) shows a slightly lower electronegative environment with one N and one O atom, thus its kinetic energy is higher compared to C(2) but lower compared to C(6) with one nitrogen as closest binding partner, and C(5) and C(9) being bound only to C or H atoms. The overall difference between C(2) and C(5), C(9) kinetic energies (binding energies) is about 5 eV. The two nitrogen and oxygen atoms show negligible chemical shifts that are not resolved in the x-ray photoelectron spectra. The same concept also applies to the interpretation of the site shift observable in the C1s to $\pi*$ resonances in the NEXAFS spectrum in Fig. 14.6.

The concept of electronegativity is only a first approximation to local electron density due to binding. Detailed calculations become necessary for quantitative statements and comparisons between different nucleobases [109]. Since the electronic structure is changing as a result of optical light absorption (for example in form of the $\pi\pi*$ excitation sketched in Fig. 14.1), the photoelectron spectrum will change. Moreover, electronic and nuclear relaxation will both change the photoelectron energies and also their amplitudes. Currently however, free electron lasers are only starting to become a useful tool for x-ray photoelectron spectroscopy in the C, N and O 1s region. Typical spectral width and shot-to-shot jitter instabilities spoil the spectral characteristics needed for this type of spectroscopy. New schemes like self seeding are on the horizon and might radically change the prospects for ultrafast soft and hard x-ray photoelectron spectroscopy for photoexcited molecular states [110, 111].

14.4 Sources for Ultrafast X-Ray Spectroscopy

Table 14.1 shows a systematic comparison of different short pulse x-ray sources. It is important to note here, that the usefulness of a particular source depends on the scientific question to be addressed, the experimental method to be implemented, the availability of beamtime, and the complexity of its operation. In general, there is no best source for all experimental schemes and circumstances. Parameters not included in the table like brilliance, longitudinal and transversal coherence as well as bandwidth might be crucial in the selection of the light source. We have chosen to include high harmonic generation and plasma emission in this scheme, although their optimal spectral range is not in the soft x-ray domain, but rather in the extreme ultraviolet for the case of harmonics and the hard x-ray (HXR) for the laser driven plasma sources.

Table 14.1 Parameters for different sources in the extreme ultraviolet and x-ray range

	HHG	Laser driven plasma	Synchrotron	FEL
Photon energy	Typically 20–100 eV—recently up to 1.5 keV at reduced flux [112]	K_α lines and bremsstrahlung of metals in hard x-ray region	Throughout EUV, SXR, HXR range	Throughout EUV, SXR, HXR at different facilities
Pulse duration	~0.1 fs to some 10 fs	>100 fs	100 fs for slicing, 1 ps for special mode, 100 ps normal	Few femtosecond to few 100 fs
Flux (photons/s)	~10^{12} @ 1 kHz	10^{10} @ 1 kHz into full solid angle	10^4–10^6 in slicing at 1 kHz, 10^9 for picoseconds pulses @ MHz [113], >10^{13} for 100 ps @ MHz	About 10^{12} per pulse at repetition rates determined by the facility

Strong field laser based harmonic sources started in the late 80's to early 90's [114–117]. Their temporal structure, interpreted as a train of attosecond pulses resulting from electron ionization and recollision [118–122], made them suitable for attosecond physics in the extreme ultraviolet domain from about 20–100 eV [123, 124]. New developments in mid-infrared laser sources have led to higher photon energies reaching up to 1.5 keV [112], however at reduced flux due to the 20 Hz repetition rate of the drive laser.

Laser driven plasma [125–127] sources are based on strong field ionization and plasma generation on a metal target. The laser accelerates electrons from a metal target and accelerates them back into the target, thereby creating incoherent emission of characteristic recombination lines as well as a bremsstrahlung continuum. The pulse duration is given by the travel time of the electrons through the metal target, which can be as short as 100 fs [128]. Those sources typically create 10^{10} photons/sec into the full spatial angle. The usable portion is given by the sample size or the collection efficiency of hard x-ray optics [129].

Slicing beamlines at synchrotron sources were pioneered in the beginning of the new century at the Advanced Light Source in Berkeley [1, 130]. Now, those beamlines are available in the soft and hard x-ray range at a few synchrotrons around the world achieving ~100 fs time accuracy with an integrated flux of 10^4–10^6 photons/sec [131–133]. At slicing beamlines, an optical laser is used for energy modulation of the synchrotron energy bunches. The modulated part consecutively emits femtosecond pulses during the interaction with bending magnets, wigglers or undulators. The optical laser, which has been used for the electron energy modulation, can be used as a perfectly synchronized sample excitation pulse. Without slicing,

synchrotrons typically deliver 100 ps time resolution, which can be further shortened into the picoseconds range [113, 134, 135]. For all laser pump-synchrotron probe experiments, the laser oscillator has to be feedback locked to the radio frequency clock of the synchrotron, as demonstrated for example in [136, 137].

Free electron laser (FEL) sources are now the brightest short pulse EUV and x-ray sources. Historically, the free electron laser in Hamburg-FLASH [2] in Germany was the first FEL in the EUV and soft x-ray domain. The Linac coherent light source (LCLS) [3] at SLAC/USA pushed the spectral range of FELs further into the soft and hard x-ray domains in 2009. The SPring-8 Angstrom Compact free electron Laser (SACLA) [4], which turned on at Riken-Harima/Japan in 2011 is currently the latest SXR/HXR FEL. Due to the high flux of 10^{12} photons/pulse at 120 Hz repetition rate for the example of LCLS, the FELs provide an enormous flexibility for different types of spectroscopy. All three sources mentioned above were designed unseeded, resulting in large pulse to pulse fluctuations in of pulse power and pulse spectrum. In the hard x-ray range, a self seeding scheme was recently accomplished at the LCLS [110]. The resulting pulses have 1/40–1/50 compared to the SASE bandwidth and are much closer to the Fourier transform limit [110]. Similar schemes are planned for narrowing and stabilizing the pulse spectra in the soft x-ray range [111]. The first operational seeded FEL is FERMI in Italy [138] and recent progress by direct seeding with EUV light was demonstrated at FLASH [139].

For seeded FELs, timing to optical excitation lasers is straightforward, since the seeding laser infrastructure can also be used for sample excitation. At unseeded FEL sources delay accuracy between optical excitation and x-ray probe pulses can be improved by additional setups which determine the delay between the two pulses on a shot to shot basis. There are two fundamentally different methods to determine the excitation—x-ray delay. The first scheme uses the fact that the optical reflectivity of a solid sample is changed if pumped by a sufficiently strong x-ray pump pulse. The physical effect was demonstrated at FLASH, and authors pointed out that a single shot tool could be built by spatially resolving the reflectivity for a non-collinear geometry of x-ray and optical probe pulse [140]. A single shot monitor based on spatial encoding was later used at LCLS [141, 142]. Higher accuracy monitors were later realized using spectral encoding by a chirped (that means temporally extended by a spectral phase) continuum and provide down to 10 fs timing accuracy [143–145]. A second scheme is based on strong field interactions with x-ray emitted electrons. When a gas phase target is x-ray ionized in the presence of a strong infrared laser field, the laser field modulates the electron kinetic energy if the pulses overlap in time [146–149]. If the few femtosecond period of the optical laser is further increased to several 100 fs by THz pulse generation, a single shot delay monitor can be accomplished since the electron kinetic energy modulation reflects the THz vector potential strength at the time of x-ray photoemission [150]. This scheme has recently been used to even determine the temporal profile of the x-ray pulses [151, 152].

14.5 Ultrafast X-Ray Probing of Photoexcited Molecular Dynamics

We now start with the discussion of ultrafast optical pump—x-ray probe experiments. The field of ultrafast x-ray molecular spectroscopy with gas phase molecules has been really opened by x-ray FELs due to the high flux needed in these experiments. The sources are young thus there are currently very few experiments.

Cryan et al. [153] had performed the first optical- pump- x-ray probe experiment at the LCLS. They used a nonresonant infrared laser pulse to align nitrogen molecules before core-ionizing them with a soft x-ray pulse. In the experiment, alignment provided means to measure angular distributions of electrons in the molecular frame. The intense and short ($<5\,\mathrm{fs}$) soft x-ray pulse created two core hole vacancies in the molecule [154–156]. This process can occur on a single atom within the molecule (single site double core hole, ssDCH) or on two different atoms (double site double core hole, dsDCH). Cryan et al. succeeded to identify the signature of the ssDCH in the high kinetic energy part of the Auger spectrum and measured the Auger electron angular dependence by varying the angle between the molecular alignment and the soft x-ray polarization.

Molecular dynamics on a UV excited molecular state was probed using soft x-ray induced fragmentation by Petrović et al. [157]. Compared to the well established technique of infrared strong field Coulomb explosion, the x-ray induced fragmentation bears several advantages. In the strong infrared field with field strength sufficient needed to ionize, other effects like alignment, bond softening, above threshold ionization, and intermediate multi-photon resonances can alter the ionization yield and kinetic energy. All these effects are negligible for soft x-ray core ionization creating two valence holes via Auger decay. The UV pump pulse triggered a ring opening reaction from cyclohexadiene to hexatriene via nonadiabatic excited state dynamics. Increasing time delay between the UV and soft x-ray pulse resulted in an increased H^+ emission. Further steady state spectroscopy on the pure compounds confirmed that the photoproduct hexatriene leads to higher proton production after soft x-ray ionization compared to cyclohexadiene.

For the case of thymine, the lifetime of the $\pi\pi^*$ state is a matter of debate. As discussed in the second section of this chapter on molecular dynamics, two different theoretical approaches predict different $\pi\pi^*$ state lifetimes based on the involvement or absence of a reaction barrier. The current ultrafast optical experiments all show very similar time constants, however they can be interpreted by both competing models. This is clearly a good motivation to investigate the molecular excited state dynamics with a fundamentally different probe, as the element selective and locally sensitive x-rays provide.

The experiment discussed in the following was performed at the LCLS by the "LCLS nucleobase collaboration" [27, 158] at the so called AMO instrument [159]. Thymine was evaporated at $150\,^\circ$C and transported into the interaction region using a hollow capillary oven [160]. An ultraviolet pulse excited thymine from the

electronic ground state to its π π* state. The time-delayed soft x-ray pulse had a pho-
ton energy above the oxygen K edge and photoionized the molecule. The oxygen 1s
Auger spectrum was energy resolved using a 2 m long magnetic bottle spectrometer
[161, 162], a spectrum was saved for every shot. In addition, the time jitter between
UV pump and soft x-ray probe pulse was determined by x-ray induced changes in the
optical reflectivity for every shot [141] as described in the preceding section. This
allowed for resorting of all single shot spectra with jitter accuracy around 70–100 fs.
More technical details of the experiment are described in [27].

Figure 14.8 shows the experimental data of the UV pump-x-ray probe scan over a
range from −0.5 to 20 ps delay. It is worth mentioning that the time points in Fig. 14.8a
are not equidistant; for small delays we have a time binning of 70 fs, the largest delays
have a relative separation of 15 ps. It is however obvious, that most change occurs
in the picosecond after the zero delay. The subtraction of unexcited spectra from
UV excited spectra reveals the change between the unexcited and excited molecule,
therefore we plot difference spectra of UV excited minus unexcited samples in part a.
Blue colors indicate a UV induced decrease of Auger electron yield and the specific
kinetic energy and delay, red indicates a UV induced increase of the Auger yield.
The signal at negative times before zero delay has a large error due to reduced data
acquisition times, which results in random color fluctuations. The first systematic
signal occurs right after zero delay at positive times. One can clearly identify a
signal decrease in kinetic energy region number II (around 500 eV kinetic energy)
that lasts for the full measurement interval. In region number I (around 507 eV kinetic
energy), we identify a short lived positive feature, which can be analyzed better in
the integrated signals plotted as a function of delay in c. The fit to the integral of
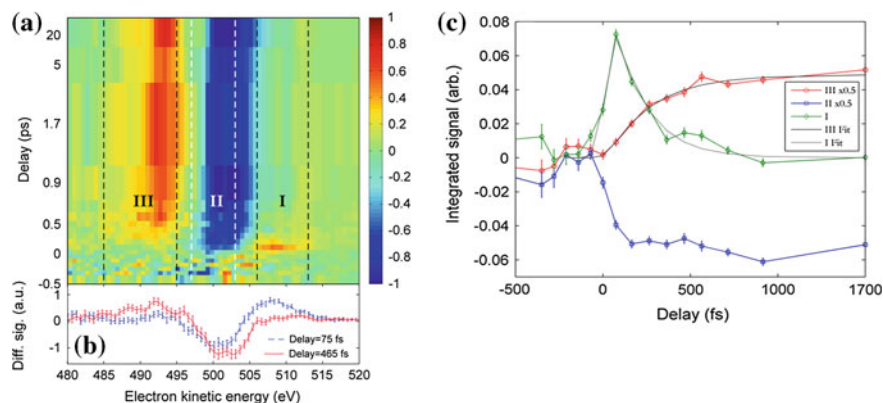

Fig. 14.8 **a** Difference Auger spectra with and without UV excitation versus time delay between
UV excitation and SXR probe pulse. The false color plot indicates the sign and amplitude of the
difference, *red* indicates a UV induced increase of the Auger yield, *blue* indicates a UV induced
Auger yield decrease. Part **b** shows difference spectra at two different delays (75 fs *dashed blue* and
465 fs *solid red*). In **c**, integrations over kinetic energy ranges indicated in (**a**) are scaled by a factor
(see legend) and fitted (see main text)

region I shows a 200 fs decay constant. The rise of region I and decay of region II is synchronous. As region I decays, the signal in region III (around 490 eV) rises with a time constant similar to the decay of I. This suggests that some kind of decay in a photoexcited state is accompanied by a rise in a product state.

A cut through the difference spectrum at short times is given in blue in Fig. 14.8b. We clearly identify the decrease in II accompanied by the increase in I. Such a difference spectrum reflects a UV induced shift of the whole ground state Auger band (see Fig. 14.7) towards higher Auger kinetic energies. The immediate appearance with UV excitation indicates the creation of a wave packet in the $\pi\pi^*$ excited state.

The reason for the blueshift of the Auger electrons upon $\pi\pi^*$ excitation lies in the nuclear dynamics of the molecule, as can be shown by comparison to simulations as done in [27]. However, the signal can as well be interpreted using intuitive arguments which are based on the x-ray typical element and local sensitivity. As explained in Sect. 14.3, the Auger decay of the oxygen 1s core holes involves orbitals with strong oxygen atomic orbital character [94, 98]. This means that the final state after Auger decay is a dicationic state with valence charge missing at one of the two oxygen atoms, indistinguishable for us. The lacking valence electrons at the oxygen are reducing the electron density between the oxygen and the next nearest carbon. Due to this effect, a strong Coulomb repulsion acts between those atoms in the dicationic state. Figure 14.9 shows a sketch of the electronic energies in the neutral $\pi\pi^*$ state, the core ionized $1s^{-1}\pi\pi^*$ state and a 'band' of dicationic states reached upon Auger decay. As the molecule elongates the C–O coordinate, the dicationic state lowers its energy considerably due to Coulomb repulsion. This results in a increase of the Auger kinetic energy for O1s core hole decay as the C–O coordinate increases.

Simulations predict that one of the two thymine C–O bonds indeed stretches as the molecule is excited to the $\pi\pi^*$ state. Upon excitation, the C(4)–O(8) bond, which is close to the methyl group, is Franck-Condon active, as explained in the context of Fig. 14.1. It elongates by about 15 % as the molecule relaxes from the Franck-Condon nuclear geometry to the predicted $\pi\pi^*$ state minimum [41, 42]. In contrast, the C(2)–O(7) bond does not change as a consequence of photoexcitation. This fast nuclear relaxation occurs immediately after the UV excitation, and the experimental time resolution is not sufficient to follow the relaxation and resolve the gradual shift. It is interesting to note that the high local sensitivity of the 1s Auger decay allows to really attribute motion to individual bonds. For the current case of thymine, it is not possible to tell from the spectra, which of the two C–O bonds stretches. As explained in Sect. 14.3, sites (here corresponding to O(7) and O(8)) cannot be identified in the broad and complex Auger spectra. For molecules with singly occurring elements however, the x-ray probe combined with Auger decay does provide an opportunity to intuitively explore excited state nuclear dynamics.

About 200 fs after photoexcitation, a decrease in region I is observed together with a rise in region III. The time delay cut at 465 fs in Fig. 14.8b shows a difference spectrum indicating UV induced shift to lower Auger kinetic energies. This is contrary to the nuclear dynamics trend described above. We evaluate the decay of the blueshifted spectrum from the $\pi\pi^*$ state in the light of past investigations. Simula-
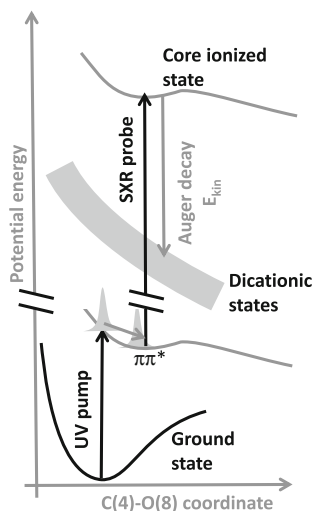
Fig. 14.9 Scheme of potential energy surfaces involved in the excited state Auger probing, plotted over the C(4)–O(8) distance. The UV excitation pulse promotes a molecular wavepacket to the $\pi\pi^*$ state. The soft x-ray pulse core ionizes the molecule creating a 1s vacancy at oxygen and leaving the valence $\pi\pi^*$ configuration intact. This core ionized state decays within a few femtoseconds to the dicationic states, which are indicated as a grey band. The kinetic energy of the Auger electron is given by the energy difference between core excited and dicationic state. The dicationic states lower the energy strongly as the C–O bond stretches. This results from the high localization of the double valence hole in the vicinity of the oxygen atom after the Auger decay. The unscreened nuclear repulsion term between O(8) and its bond partner C(4) decreases as the C–O bond stretches, explaining the Auger blueshift from Franck-Condon region to $\pi\pi^*$ minimum

tions in [41, 42] predict that the molecule is stuck on a minimum in the $\pi\pi^*$ state for some picoseconds due to a reaction barrier in the path to reach the conical intersection. The C(4)–O(8) bond stays elongated in this minimum. Thus these simulations would predict a blueshifted spectrum for the next couple of picoseconds after excitation. The experimentally observed decay of the blueshifted channel with 200 fs time constant indicates that this minimum can only live for a short time <200 fs. Thus, we assume that the majority of the photoexcited $\pi\pi^*$ population is not blocked by a barrier and has quick access to the conical intersection region. The redshift can only be explained by considering a transition to a different electronic state. The shift is than induced either by the C–O bond shrinking or a changed electronic structure.

A return of photoexcited population to the vibrationally hot ground state as well as population of the dark $n\pi^*$ state is possible and was controversially discussed in the theoretical literature [41, 42, 53–55]. Simulations of Auger spectra in [27] show a redshift for the $n\pi^*$ state and no shift but rather a slight broadening for a return to the hot ground state. While relaxation to the $n\pi^*$ state can explain the experimental redshift, a statement on ground state relaxation is not possible. Our simulated ground state spectra indicate that the x-ray Auger method has reduced sensitivity on the ground state relaxation channel.

Short decay constants, comparable to the 200 fs trace, have been documented in the optical pump-probe literature [66–68] and were interpreted either as nuclear relaxation on the π π* state or electronic relaxation out of this state. The soft x-ray Auger experiment distinguishes between nuclear and electronic relaxation and we can interpret the 200 fs decrease in region I as an *electronic* reduction of the π π* population. The fast decay of a majority of the π π* state population means barrier-less decay of the π π* state. Several simulations point towards the hot ground state as a product of few 100 fs electronic relaxation [53, 54], which was confirmed in liquid phase [163]. Due to reduced Auger sensitivity to this state, we abstain from a statement. The time constant of the lower energy signal indicates a 200–300 fs filling of the nπ* state. In order to show excited state fluorescence as measured in liquid phase according to [164], some molecular population must be trapped behind a π π* reaction barrier. We assume that experimental signal to noise ratio in the x-ray Auger experiment is not yet good enough to deduce such detailed information.

14.6 Outlook

We are only at the beginning of investigating photoexcited molecular dynamics with ultrashort x-ray pulses. The couple of experiments done in the past showed the promise of the field, which is element and site selective probing of valence dynamics. Many more systematic experiments are needed to fully appreciate the strength and weakness of ultrafast x-ray probing and to position it in the context of other ultrafast techniques.

Several exciting new methodological developments are of crucial importance for this new field. Powerful x-ray pulses can now be delivered with stable bandwidth due to self-seeding schemes [110, 111], which enables femtosecond core electron photoemission for molecular dynamics probing. In addition, techniques relying on hitting molecular core-valence resonances will be profiting to a great extend. Having sources with higher average repetition rate like to European XFEL [165] will make emission experiments in dilute samples feasible. In addition, new nonlinear x-ray methods are currently getting developed on the theoretical side for molecular systems [166–169] and at the same time first FEL induced lasing and Raman processes in atoms have shown that these methods can also be translated into an experiment [170, 171]. We currently witness a fast growth in available FEL beamtime as more lasers are coming online in the near future in Germany [165], Switzerland [172] and Korea [173]. At the same time, the existing facilities are becoming more versatile. This should deliver ideal conditions for a broad molecular science program at free electron lasers.

References

1. R. Schoenlein, S. Chattopadhyay, H. Chong, T. Glover, P. Heimann, C. Shank, A. Zholents, M. Zolotorev, Science **287**, 2237 (2000)
2. W. Ackermann, G. Asova, V. Ayvazyan, A. Azima, N. Baboi, J. Baehr, V. Balandin, B. Beutner, A. Brandt, A. Bolzmann, R. Brinkmann, O.I. Brovko, M. Castellano, P. Castro, L. Catani, E. Chiadroni, S. Choroba, A. Cianchi, J.T. Costello, D. Cubaynes, J. Dardis, W. Decking, H. Delsim-Hashemi, A. Delserieys, G. Di Pirro, M. Dohlus, S. Duesterer, A. Eckhardt, H.T. Edwards, B. Faatz, J. Feldhaus, K. Floettmann, J. Frisch, L. Froehlich, T. Garvey, U. Gensch, C. Gerth, M. Goerler, N. Golubeva, H.-J. Grabosch, M. Grecki, O. Grimm, K. Hacker, U. Hahn, J.H. Han, K. Honkavaara, T. Hott, M. Huening, Y. Ivanisenko, E. Jaeschke, W. Jalmuzna, T. Jezynski, R. Kammering, V. Katalev, K. Kavanagh, E.T. Kennedy, S. Khodyachykh, K. Klose, V. Kocharyan, M. Koerfer, M. Kollewe, W. Koprek, S. Korepanov, D. Kostin, M. Krassilnikov, G. Kube, M. Kuhlmann, C.L.S. Lewis, L. Lilje, T. Limberg, D. Lipka, F. Loehl, H. Luna, M. Luong, M. Martins, M. Meyer, P. Michelato, V. Miltchev, W.D. Moeller, L. Monaco, W.F.O. Mueller, A. Napieralski, O. Napoly, P. Nicolosi, D. Noelle, T. Nunez, A. Oppelt, C. Pagani, R. Paparella, N. Pchalek, J. Pedregosa-Gutierrez, B. Petersen, B. Petrosyan, G. Petrosyan, L. Petrosyan, J. Pflueger, E. Ploenjes, L. Poletto, K. Pozniak, E. Prat, D. Proch, P. Pucyk, P. Radcliffe, H. Redlin, K. Rehlich, M. Richter, M. Roehrs, J. Roensch, R. Romaniuk, M. Ross, J. Rossbach, V. Rybnikov, M. Sachwitz, E.L. Saldin, W. Sandner, H. Schlarb, B. Schmidt, M. Schmitz, P. Schmueser, J.R. Schneider, E.A. Schneidmiller, S. Schnepp, S. Schreiber, M. Seidel, D. Sertore, A.V. Shabunov, C. Simon, S. Simrock, E. Sombrowski, A.A. Sorokin, P. Spanknebel, R. Spesyvtsev, L. Staykov, B. Steffen, F. Stephan, F. Stulle, H. Thom, K. Tiedtke, M. Tischer, S. Toleikis, R. Treusch, D. Trines, I. Tsakov, E. Vogel, T. Weiland, H. Weise, M. Wellhoeffer, M. Wendt, I. Will, A. Winter, K. Wittenburg, W. Wurth, P. Yeates, M.V. Yurkov, I. Zagorodnov, K. Zapfe, Nat. Photonics **1**, 336 (2007)
3. P. Emma, R. Akre, J. Arthur, R. Bionta, C. Bostedt, J. Bozek, A. Brachmann, P. Bucksbaum, R. Coffee, F.-J. Decker, Y. Ding, D. Dowell, S. Edstrom, A. Fisher, J. Frisch, S. Gilevich, J. Hastings, G. Hays, P. Hering, Z. Huang, R. Iverson, H. Loos, M. Messerschmidt, A. Miahnahri, S. Moeller, H.-D. Nuhn, G. Pile, D. Ratner, J. Rzepiela, D. Schultz, T. Smith, P. Stefan, H. Tompkins, J. Turner, J. Welch, W. White, J. Wu, G. Yocky, J. Galayda, Nat. Photonics **4**, 641 (2010)
4. T. Ishikawa, H. Aoyagi, T. Asaka, Y. Asano, N. Azumi, T. Bizen, H. Ego, K. Fukami, T. Fukui, Y. Furukawa, S. Goto, H. Hanaki, T. Hara, T. Hasegawa, T. Hatsui, A. Higashiya, T. Hirono, N. Hosoda, M. Ishii, T. Inagaki, Y. Inubushi, T. Itoga, Y. Joti, M. Kago, T. Kameshima, H. Kimura, Y. Kirihara, A. Kiyomichi, T. Kobayashi, C. Kondo, T. Kudo, H. Maesaka, X.M. Maréchal, T. Masuda, S. Matsubara, T. Matsumoto, T. Matsushita, S. Matsui, M. Nagasono, N. Nariyama, H. Ohashi, T. Ohata, T. Ohshima, S. Ono, Y. Otake, C. Saji, T. Sakurai, T. Sato, K. Sawada, T. Seike, K. Shirasawa, T. Sugimoto, S. Suzuki, S. Takahashi, H. Takebe, K.

Takeshita, K. Tamasaku, H. Tanaka, R. Tanaka, T. Tanaka, T. Togashi, K. Togawa, A. Tokuhisa, H. Tomizawa, K. Tono, S. Wu, M. Yabashi, M. Yamaga, A. Yamashita, K. Yanagida, C. Zhang, T. Shintake, H. Kitamura, N. Kumagai, Nat. Photonics **6**, 540 (2012)

5. J. Ullrich, A. Rudenko, R. Moshammer, Annu. Rev. Phys. Chem. **63**, 635 (2012)
6. F. Plasser, M. Barbatti, A.J.A. Aquino, H. Lischka, Theor. Chem. Acc. **131**, 233902 (2012)
7. J.C. Tully, J. Chem. Phys. **137**, 22A301 (2012)
8. H. Dürr, H. Bouas-Laurent (eds.), *Photochromism: Molecules and Systems*, Rev edn. (Elsevier, Boston, 2003)
9. M. Alemani, M.V. Peters, S. Hecht, K.-H. Rieder, F. Moresco, L. Grill, J. Am. Chem. Soc. **128**, 14446 (2006)
10. M. Comstock, N. Levy, A. Kirakosian, J. Cho, F. Lauterwasser, J. Harvey, D. Strubbe, J. Fréchet, D. Trauner, S. Louie, M. Crommie, Phys. Rev. Lett. **99**, 038301 (2007)
11. R.J. Sension, S.T. Repinec, A.Z. Szarka, R.M. Hochstrasser, J. Chem. Phys. **98**, 6291 (1993)
12. D.H. Waldeck, Chem. Rev. **91**, 415 (1991)
13. R. Schoenlein, L. Peteanu, R. Mathies, C. Shank, Science **254**, 412 (1991)
14. D. Polli, P. Altoe, O. Weingart, K.M. Spillane, C. Manzoni, D. Brida, G. Tomasello, G. Orlandi, P. Kukura, R.A. Mathies, G. Cerullo, Nature **467**, 440 (2010)
15. R. Mathies, C. Brito Cruz, W. Pollard, C. Shank, Science **240**, 777 (1988)
16. S. Schenkl, F. van Mourik, G. van der Zwan, S. Haacke, M. Chergui, Science **309**, 917 (2005)
17. G. Groenhof, M. Bouxin-Cademartory, B. Hess, S.P. de Visser, H.J.C. Berendsen, M. Olivucci, A.E. Mark, M.A. Robb, J. Am. Chem. Soc. **126**, 4228 (2004)
18. C.T. Middleton, K. de La Harpe, C. Su, Y.K. Law, C.E. Crespo-Hernandez, B. Kohler, Annu. Rev. Phys. Chem. **60**, 217 (2009)
19. C. Crespo-Hernandez, B. Cohen, P. Hare, B. Kohler, Chem. Rev. **104**, 1977 (2004)
20. W.J. Schreier, T.E. Schrader, F.O. Koller, P. Gilch, C.E. Crespo-Hernandez, V.N. Swaminathan, T. Carell, W. Zinth, B. Kohler, Science **315**, 625 (2007)
21. E. Teller, Isr. J. Chem. **7**, 227 (1969)
22. H. Köppel, W. Domcke, L.S. Cederbaum, Adv. Chem. Phys. **57**, 59 (1984)
23. F. Bernardi, M. Olivucci, M.A. Robb, Chem. Soc. Rev. **25**, 321 (1996)
24. G.A. Worth, L.S. Cederbaum, Annu. Rev. Phys. Chem. **55**, 127 (2004)
25. W. Domcke, D. Yarkony, H. Köppel (eds.), *Conical Intersections Electronic Structure, Dynamics & Spectroscopy* (World Scientific, River Edge, 2004)
26. R. Dörner, V. Mergel, O. Jagutzki, L. Spielberger, J. Ullrich, R. Moshammer, H. Schmidt-Bocking, Phys. Rep.-Rev. Sect. Phys. Lett. **330**, 95 (2000)
27. B.K. McFarland, J.P. Farrell, S. Miyabe, F. Tarantelli, A. Aguilar, N. Berrah, C. Bostedt, J.D. Bozek, P.H. Bucksbaum, J.C. Castagna, R.N. Coffee, J.P. Cryan, L. Fang, R. Feifel, K.J. Gaffney, J.M. Glownia, T.J. Martinez, M. Mucke, B. Murphy, A. Natan, T. Osipov, V.S. Petrović, S. Schorb, T. Schultz, L.S. Spector, M. Swiggers, I. Tenney, S. Wang, J.L. White, W. White, M. Gühr, Nat. Commun. **5**, 4235 (2014)
28. M. Born, R. Oppenheimer, Ann. Phys. **389**, 457 (1927)
29. W. Domcke, D.R. Yarkony, H. Köppel (eds.), *Conical Intersections Theory*, Computation and Experiment (World Scientific Publishing Company, Singapore, 2011)
30. B.L. Henke, E.M. Gullikson, J.C. Davis, At. Data Nucl. Data Tables **54**, 181 (1993)
31. J.J. Yeh, I. Lindau, At. Data Nucl. Data Tables **32**, 1 (1985)
32. K. Siegbahn, *ESCA Applied to Free Molecules* (North-Holland Pub. Co, Amsterdam, 1969)
33. P.S. Bagus, F. Illas, G. Pacchioni, F. Parmigiani, J. Electron Spectrosc. Relat. Phenom. **100**, 215 (1999)
34. R. Manne, J. Chem. Phys. **52**, 5733 (1970)
35. J.M. Coxon, *Organic Photochemistry* (Cambridge University Press, New York, 1974)
36. M. Klessinger, *Excited States and Photochemistry of Organic Molecules* (VCH, New York, 1995)
37. J. Michl, V. Bonačić-Koutecký, Electronic Aspects of Organic Photochemistry (Wiley, New York, 1990)
38. N.J. Turro, Modern Molecular Photochemistry (University Science Books, Mill Valley, 1991)

39. R. Mulliken, Phys. Rev. **46**, 549 (1934)
40. R.S. Mulliken, J. Chem. Phys. **55**, 288 (1971)
41. H.R. Hudock, B.G. Levine, A.L. Thompson, H. Satzger, D. Townsend, N. Gador, S. Ullrich, A. Stolow, T.J. Martínez, J. Phys. Chem. A **111**, 8500 (2007)
42. J.J. Szymczak, M. Barbatti, J.T. Soo, Hoo, J.A. Adkins, T.L. Windus, D. Nachtigallova, H. Lischka, J. Phys. Chem. A **113**, 12686 (2009)
43. D.J. Tannor, *Introduction to Quantum Mechanics: A Time-Dependent Perspective* (University Science Books, Sausalito, 2007)
44. J. Yeazell, T. Uzer (eds.), *The Physics and Chemistry of Wave Packets* (Wiley, New York, 2000)
45. M. Gühr, H. Ibrahim, N. Schwentner, Phys. Chem. Chem. Phys. **6**, 5353 (2004)
46. D.J. Nesbitt, R.W. Field, J. Phys. Chem. **100**, 12735 (1996)
47. G. Herzberg, Molecular Spectra and Molecular Structure: Infrared and Raman Spectra of Polyatomic Molecules (R.E. Krieger Pub. Co., Malabar, 1991)
48. D. Yarkony, Rev. Mod. Phys. **68**, 985 (1996)
49. E. Teller, J. Phys. Chem. **41**, 109 (1937)
50. B.G. Levine, T.J. Martínez, Annu. Rev. Phys. Chem. **58**, 613 (2007)
51. G.J. Atchity, S.S. Xantheas, K. Ruedenberg, J. Chem. Phys. **95**, 1862 (1991)
52. T.J. Martínez, Nature **467**, 412 (2010)
53. M. Merchán, R. González-Luque, T. Climent, L. Serrano-Andrés, E. Rodríguez, M. Reguero, D. Peláez, J. Phys. Chem. B **110**, 26471 (2006)
54. S. Perun, A.L. Sobolewski, W. Domcke, J. Phys. Chem. A **110**, 13238 (2006)
55. D. Asturiol, B. Lasorne, M.A. Robb, L. Blancafort, J. Phys. Chem. A **113**, 10211 (2009)
56. A.H. Zewail (ed.), *Femtochemistry: Ultrafast Dynamics of the Chemical Bond* (World Scientific, River Edge, 1994)
57. T. Baumert, M. Grosser, R. Thalweiser, G. Gerber, Phys. Rev. Lett. **67**, 3753 (1991)
58. M. Spanner, S. Patchkovskii, C. Zhou, S. Matsika, M. Kotur, T.C. Weinacht, Phys. Rev. A **86**, 053406 (2012)
59. B.K. McFarland, J.P. Farrell, P.H. Bucksbaum, M. Gühr, Science **322**, 1232 (2008)
60. A. Stolow, Annu. Rev. Phys. Chem. **54**, 89 (2003)
61. A. Stolow, A.E. Bragg, D.M. Neumark, Chem. Rev. **104**, 1719 (2004)
62. V. Blanchet, M. Zgierski, T. Seideman, A. Stolow, Nature **401**, 52 (1999)
63. V. Blanchet, S. Lochbrunner, M. Schmitt, J. Shaffer, J. Larsen, M. Zgierski, T. Seideman, A. Stolow, Faraday Discuss. **115**, 33 (2000)
64. I.V. Hertel, W. Radloff, Rep. Prog. Phys. **69**, 1897 (2006)
65. M. Barbatti, S. Ullrich, Phys. Chem. Chem. Phys. **13**, 15492 (2011)
66. H. Kang, K.T. Lee, B. Jung, Y.J. Ko, S.K. Kim, J. Am. Chem. Soc. **124**, 12958 (2002)
67. C. Canuel, M. Mons, F. Piuzzi, B. Tardivel, I. Dimicoli, M. Elhanine, J. Chem. Phys. **122**, 074316 (2005)
68. J. González-Vázquez, L. González, E. Samoylova, T. Schultz, Phys. Chem. Chem. Phys. **11**, 3927 (2009)
69. S. Ullrich, T. Schultz, M.Z. Zgierski, A. Stolow, Phys. Chem. Chem. Phys. **6**, 2796 (2004)
70. A.P. Hitchcock, J. Electron Spectrosc. Relat. Phenom. **67**, 1 (1994)
71. E.D. Palik, *Handbook of Optical Constants of Solids* (Academic Press, New York, 1998)
72. K. Ueda, J. Phys. B At. Mol. Opt. Phys. **36**, R1 (2003)
73. U. Becker, D.A. Shirley (eds.), *VUV and Soft X-Ray Photoionization* (Plenum Press, New York, 1996)
74. J. Stöhr, NEXAFS Spectroscopy, 1st edn. corr. print (Springer, New York, 1996)
75. A. Nilsson, L.G.M. Pettersson, in *Chemical Bonding at Surfaces and Interfaces*, ed. by A. Nilsson, L.G.M. Pettersson, J. Norskov (Elsevier Science, Amsterdam, 2011)
76. S. Schreck, G. Gavrila, C. Weniger, P. Wernet, Rev. Sci. Instrum. **82**, 103101 (2011)
77. M. Ukai, A. Yokoya, K. Fujii, Y. Saitoh, Chem. Phys. Lett. **495**, 90 (2010)
78. J. Nordgren, New Directions in Research with Third-Generation Soft X-Ray Synchrotron Radiation Sources (Kluwer Academic, Boston, 1994)

79. O. Plekan, V. Feyer, R. Richter, M. Coreno, M. de Simone, K.C. Prince, A.B. Trofimov, E.V. Gromov, I.L. Zaytseva, J. Schirmer, Chem. Phys. **347**, 360 (2008)
80. J.L. Dehmer, J. Chem. Phys. **56**, 4496 (1972)
81. D. Dill, J. Dehmer, J. Chem. Phys. **61**, 692 (1974)
82. J. Dehmer, D. Dill, Phys. Rev. Lett. **35**, 213 (1975)
83. J.L. Dehmer, D. Dill, J. Chem. Phys. **65**, 5327 (1976)
84. W. Wurth, J. Stöhr, Vacuum **41**, 237 (1990)
85. W. Bambynek, B. Crasemann, R. Fink, H. Freund, H. Mark, C. Swift, R. Price, P. Rao, Rev. Mod. Phys. **44**, 716 (1972)
86. P. Glatzel, U. Bergmann, Coord. Chem. Rev. **249**, 65 (2005)
87. J. Nordgren, G. Bray, S. Cramm, R. Nyholm, J.-E. Rubensson, N. Wassdahl, Rev. Sci. Instrum. **60**, 1690 (1989)
88. P. Glans, P. Skytt, K. Gunnelin, J.-H. Guo, J. Nordgren, J. Electron Spectrosc. Relat. Phenom. **82**, 193 (1996)
89. P. Glans, K. Gunnelin, P. Skytt, J.-H. Guo, N. Wassdahl, J. Nordgren, H. Ågren, F. Gel'mukhanov, T. Warwick, E. Rotenberg, Phys. Rev. Lett. **76**, 2448 (1996)
90. P. Skytt, P. Glans, K. Gunnelin, J. Guo, J. Nordgren, Y. Luo, H. Ågren, Phys. Rev. A **55**, 134 (1997)
91. A. Cesar, F. Gel'mukhanov, Y. Luo, H. Ågren, P. Skytt, P. Glans, J. Guo, K. Gunnelin, J. Nordgren, J. Chem. Phys. **106**, 3439 (1997)
92. I. Josefsson, K. Kunnus, S. Schreck, A. Föhlisch, F. de Groot, P. Wernet, M. Odelius, J. Phys. Chem. Lett. **3**, 3565 (2012)
93. Y. Harada, T. Takeuchi, H. Kino, A. Fukushima, K. Takakura, K. Hieda, A. Nakao, S. Shin, H. Fukuyama, J. Phys. Chem. A **110**, 13227 (2006)
94. H. Siegbahn, L. Asplund, P. Kelfve, Chem. Phys. Lett. **35**, 330 (1975)
95. E.H.S. Burhop, *The Auger Effect and Other Radiationless Transitions* (R. E. Krieger Pub. Co, Huntington, 1980)
96. P. Emma, K. Bane, M. Cornacchia, Z. Huang, H. Schlarb, G. Stupakov, D. Walz, Phys. Rev. Lett. **92**, 074801 (2004)
97. W.E. Moddeman, T.A. Carlson, M.O. Krause, B.P. Pullen, W.E. Bull, G.K. Schweitz, J. Chem. Phys. **55**, 2317 (1971)
98. L. Karlsson, L.O. Werme, T. Bergmark, K. Siegbahn, J. Electron Spectrosc. Relat. Phenom. **3**, 181 (1974)
99. H. Ågren, J. Chem. Phys. **75**, 1267 (1981)
100. L. Storchi, F. Tarantelli, S. Veronesi, P. Bolognesi, E. Fainelli, L. Avaldi, J. Chem. Phys. **129**, 154309 (2008)
101. J. Schirmer, A. Barth, Z. Fuer. Phys. At. Nucl. **317**, 267 (1984)
102. F. Tarantelli, Chem. Phys. **329**, 11 (2006)
103. W. Eberhardt, T. Sham, R. Carr, S. Krummacher, M. Strongin, S. Weng, D. Wesner, Phys. Rev. Lett. **50**, 1038 (1983)
104. E. Itälä, D.T. Ha, K. Kooser, M.A. Huels, E. Rachlew, E. Nõmmiste, U. Joost, E. Kukk, J. Electron Spectrosc. Relat. Phenom. **184**, 119 (2011)
105. E. Itälä, D.T. Ha, K. Kooser, E. Nõmmiste, U. Joost, E. Kukk, Int. J. Mass Spectrom. **306**, 82 (2011)
106. S. Hüfner, *Photoelectron Spectroscopy: Principles and Applications*, 3rd edn. (Springer, New York, 2003)
107. W.L. Jolly, K.D. Bomben, C.J. Eyermann, At. Data Nucl. Data Tables **31**, 433 (1984)
108. L.J. Sæthre, K.J. Børve, T.D. Thomas, J. Electron Spectrosc. Relat. Phenom. **183**, 2 (2011)
109. Y. Takahata, A.K. Okamoto, D.P. Chong, Int. J. Quantum Chem. **106**, 2581 (2006)
110. J. Amann, W. Berg, V. Blank, F.-J. Decker, Y. Ding, P. Emma, Y. Feng, J. Frisch, D. Fritz, J. Hastings, Z. Huang, J. Krzywinski, R. Lindberg, H. Loos, A. Lutman, H.-D. Nuhn, D. Ratner, J. Rzepiela, D. Shu, Y. Shvyd'ko, S. Spampinati, S. Stoupin, S. Terentyev, E. Trakhtenberg, D. Walz, J. Welch, J. Wu, A. Zholents, D. Zhu, Nat. Photonics **6**, 693 (2012)

111. D. Cocco, R. Abela, J.W. Amann, K. Chow, P.J. Emma, Y. Feng, G.L. Gassner, J. Hastings, P. Heimann, Z. Huang, H. Loos, P.A. Montanez, D. Morton, H.-D. Nuhn, D.F. Ratner, L.N. Rodes, U. Flechsig, J.J. Welch, J. Wu, ed. by A. Klisnick, C.S. Menoni, *Proceedings SPIE 8849 X-Ray Lasers Coherent X-Ray Sources: Development and Applications*, vol. X, p. 88490A (2013)
112. T. Popmintchev, M.-C. Chen, D. Popmintchev, P. Arpin, S. Brown, S. Alisauskas, G. Andriukaitis, T. Balciunas, O.D. Mucke, A. Pugzlys, A. Baltuska, B. Shim, S.E. Schrauth, A. Gaeta, C. Hernandez-Garcia, L. Plaja, A. Becker, A. Jaron-Becker, M.M. Murnane, H.C. Kapteyn, Science **336**, 1287 (2012)
113. R. Reininger, D.J. Keavney, M. Borland, L. Young, J. Synchrotron Radiat. **20**, 654 (2013)
114. A. McPherson, G. Gibson, H. Jara, U. Johann, T.S. Luk, I.A. McIntyre, K. Boyer, C.K. Rhodes, J. Opt. Soc. Am. B **4**, 595 (1987)
115. M. Ferray, A. L'Huillier, X.F. Li, L.A. Lompre, G. Mainfray, C. Manus, J. Phys. B At. Mol. Opt. Phys. **21**, L31 (1988)
116. J.J. Macklin, J.D. Kmetec, C.L. Gordon, Phys. Rev. Lett. **70**, 766 (1993)
117. A. L'Huillier, P. Balcou, Phys. Rev. Lett. **70**, 774 (1993)
118. J.L. Krause, K.J. Schafer, K.C. Kulander, Phys. Rev. Lett. **68**, 3535 (1992)
119. K.C. Kulander, K.J. Schafer, J.L. Krause, Laser Phys. **3**, 359 (1993)
120. K.J. Schafer, B. Yang, L.F. DiMauro, K.C. Kulander, Phys. Rev. Lett. **70**, 1599 (1993)
121. P.B. Corkum, Phys. Rev. Lett. **71**, 1994 (1993)
122. M. Lewenstein, P. Balcou, M.Y. Ivanov, A. L'Huillier, P.B. Corkum, Phys. Rev. A **49**, 2117 (1994)
123. P.B. Corkum, F. Krausz, Nat. Phys. **3**, 381 (2007)
124. F. Krausz, M. Ivanov, Rev. Mod. Phys. **81**, 163 (2009)
125. C. Rose-Petruck, R. Jimenez, T. Guo, A. Cavalleri, C.W. Siders, F. Rksi, J.A. Squier, B.C. Walker, K.R. Wilson, C.P.J. Barty, Nature **398**, 310 (1999)
126. K. Sokolowski-Tinten, C. Blome, J. Blums, A. Cavalleri, C. Dietrich, A. Tarasevitch, I. Uschmann, E. Förster, M. Kammler, M. Horn-von-Hoegen, D. von der Linde, Nature **422**, 287 (2003)
127. M. Bargheer, N. Zhavoronkov, Y. Gritsai, J.C. Woo, D.S. Kim, M. Woerner, T. Elsaesser, Science **306**, 1771 (2004)
128. M. Bargheer, N. Zhavoronkov, M. Woerner, T. Elsaesser, Chem. Phys. Chem. **7**, 783 (2006)
129. M. Bargheer, N. Zhavoronkov, R. Bruch, H. Legall, H. Stiel, M. Woerner, T. Elsaesser, Appl. Phys. B **80**, 715 (2005)
130. A. Zholents, M. Zolotorev, Phys. Rev. Lett. **76**, 912 (1996)
131. S. Khan, K. Holldack, T. Kachel, R. Mitzner, T. Quast, Phys. Rev. Lett. **97**, 074801 (2006)
132. A. Streun, A. Al-Adwan, P. Beaud, M. Böge, G. Ingold, S. Johnson, A. Keller, T. Schilcher, V. Schlott, T. Schmidt, EPAC, p. 3427 (2006)
133. P. Prigent, P. Hollander, M. Labat, M.E. Couprie, J.L. Marlats, C. Laulhé, J. Luning, T. Moreno, P. Morin, A. Nadji, F. Polack, S. Ravy, M. Silly, F. Sirotti, J. Phys. Conf. Ser. **425**, 072022 (2013)
134. J. Feikes, K. Holldack, P. Kuske, G. Wustefeld, Proceedings of Ninth European Particle Accelerator Conference EPAC04, Lucerne, CH, pp. 2287–2289 (2004)
135. X. Huang, J. Safranek, J. Corbett, Y. Nosochkov, J. Sebek, A. Terebilo, 2007 IEEE Particle Accelerator Conference, vols. 1–11, IEEE, 345 E 47th St, New York, NY 10017 USA, pp. 3507–3509 (2007)
136. E.M. Dufresne, B. Adams, M. Chollet, R. Harder, Y. Li, H. Wen, S.J. Leake, L. Beitra, X. Huang, I.K. Robinson, Nucl. Instrum. Methods Phys. Res. Sect. Accel. Spectrometers Detect. Assoc. Equip. **649**, 191 (2011)
137. H. Navirian, R. Shayduk, W. Leitenberger, J. Goldshteyn, P. Gaal, M. Bargheer, Rev. Sci. Instrum. **83**, 063303 (2012)
138. E. Allaria, R. Appio, L. Badano, W.A. Barletta, S. Bassanese, S.G. Biedron, A. Borga, E. Busetto, D. Castronovo, P. Cinquegrana, S. Cleva, D. Cocco, M. Cornacchia, P. Craievich, I. Cudin, G. D'Auria, M. Dal Forno, M.B. Danailov, R. De Monte, G. De Ninno, P. Delgiusto,

A. Demidovich, S. Di Mitri, B. Diviacco, A. Fabris, R. Fabris, W. Fawley, M. Ferianis, E. Ferrari, S. Ferry, L. Froehlich, P. Furlan, G. Gaio, F. Gelmetti, L. Giannessi, M. Giannini, R. Gobessi, R. Ivanov, E. Karantzoulis, M. Lonza, A. Lutman, B. Mahieu, M. Milloch, S.V. Milton, M. Musardo, I. Nikolov, S. Noe, F. Parmigiani, G. Penco, M. Petronio, L. Pivetta, M. Predonzani, F. Rossi, L. Rumiz, A. Salom, C. Scafuri, C. Serpico, P. Sigalotti, S. Spampinati, C. Spezzani, M. Svandrlik, C. Svetina, S. Tazzari, M. Trovo, R. Umer, A. Vascotto, M. Veronese, R. Visintini, M. Zaccaria, D. Zangrando, M. Zangrando, Nat. Photonics **6**, 699 (2012)

139. S. Ackermann, A. Azima, S. Bajt, J. Bödewadt, F. Curbis, H. Dachraoui, H. Delsim-Hashemi, M. Drescher, S. Düsterer, B. Faatz, M. Felber, J. Feldhaus, E. Hass, U. Hipp, K. Honkavaara, R. Ischebeck, S. Khan, T. Laarmann, C. Lechner, T. Maltezopoulos, V. Miltchev, M. Mittenzwey, M. Rehders, J. Rönsch-Schulenburg, J. Rossbach, H. Schlarb, S. Schreiber, L. Schroedter, M. Schulz, S. Schulz, R. Tarkeshian, M. Tischer, V. Wacker, M. Wieland, Phys. Rev. Lett. **111**, 114801 (2013)
140. C. Gahl, A. Azima, M. Beye, M. Deppe, K. Doebrich, U. Hasslinger, F. Hennies, A. Melnikov, M. Nagasono, A. Pietzsch, M. Wolf, W. Wurth, A. Foehlisch, Nat. Photonics **2**, 165 (2008)
141. S. Schorb, T. Gorkhover, J.P. Cryan, J.M. Glownia, M.R. Bionta, R.N. Coffee, B. Erk, R. Boll, C. Schmidt, D. Rolles, A. Rudenko, A. Rouzee, M. Swiggers, S. Carron, J.-C. Castagna, J.D. Bozek, M. Messerschmidt, W.F. Schlotter, C. Bostedt, Appl. Phys. Lett. **100**, 121107 (2012)
142. M. Beye, O. Krupin, G. Hays, A.H. Reid, D. Rupp, S. de Jong, S. Lee, W.-S. Lee, Y.-D. Chuang, R. Coffee, J.P. Cryan, J.M. Glownia, A. Foehlisch, M.R. Holmes, A.R. Fry, W.E. White, C. Bostedt, A.O. Scherz, H.A. Durr, W.F. Schlotter, Appl. Phys. Lett. **100**, 121108 (2012)
143. M.R. Bionta, H.T. Lemke, J.P. Cryan, J.M. Glownia, C. Bostedt, M. Cammarata, J.-C. Castagna, Y. Ding, D.M. Fritz, A.R. Fry, J. Krzywinski, M. Messerschmidt, S. Schorb, M.L. Swiggers, R.N. Coffee, Opt. Express **19**, 21855 (2011)
144. M.R. Bionta, D. French, J.P. Cryan, J.M. Glownia, N. Hartmann, D.J. Nicholson, K. Baker, C. Bostedt, M. Cammarata, M. Chollet, Y. Ding, D.M. Fritz, S.M. Durbin, Y. Feng, M. Harmand, A.R. Fry, D.J. Kane, J. Krzywinski, H.T. Lemke, M. Messerschmidt, D.F. Ratner, S. Schorb, S. Toleikis, D. Zhu, W.E. White, R.N. Coffee, S.P. Moeller, M. Yabashi, S.P. Hau-Riege (Eds.), *Proceedings SPIE*, vol. 8504, p. 85040M (2012)
145. M. Harmand, R. Coffee, M.R. Bionta, M. Chollet, D. French, D. Zhu, D.M. Fritz, H.T. Lemke, N. Medvedev, B. Ziaja, S. Toleikis, M. Cammarata, Nat. Photonics **7**, 215 (2013)
146. M. Meyer, D. Cubaynes, P. O'Keeffe, H. Luna, P. Yeates, E.T. Kennedy, J.T. Costello, P. Orr, R. Taieb, A. Maquet, S. Duesterer, P. Radcliffe, H. Redlin, A. Azima, E. Ploenjes, J. Feldhaus, Phys. Rev. A **74**, 011401 (2006)
147. M. Meyer, D. Cubaynes, J. Dardis, P. Hayden, P. Hough, V. Richardson, E.T. Kennedy, J.T. Costello, S. Duesterer, W.B. Li, P. Radcliffe, H. Redlin, J. Feldhaus, S.I. Strakhova, E.V. Gryzlova, A.N. Grum-Grzhimailo, R. Taieb, A. Maquete, J. Electron. Spectrosc. Relat. Phenom. **181**, 111 (2010)
148. S. Düsterer, P. Radcliffe, C. Bostedt, J. Bozek, A.L. Cavalieri, R. Coffee, J.T. Costello, D. Cubaynes, L.F. DiMauro, Y. Ding, G. Doumy, F. Grüner, W. Helml, W. Schweinberger, R. Kienberger, A.R. Maier, M. Messerschmidt, V. Richardson, C. Roedig, T. Tschentscher, M. Meyer, New J. Phys. **13**, 093024 (2011)
149. M. Meyer, P. Radcliffe, T. Tschentscher, J.T. Costello, A.L. Cavalieri, I. Grguras, A.R. Maier, R. Kienberger, J. Bozek, C. Bostedt, S. Schorb, R. Coffee, M. Messerschmidt, C. Roedig, E. Sistrunk, L.F. Di Mauro, G. Doumy, K. Ueda, S. Wada, S. Düsterer, A.K. Kazansky, N.M. Kabachnik, Phys. Rev. Lett. **108**, 063007 (2012)
150. U. Frühling, M. Wieland, M. Gensch, T. Gebert, B. Schuette, M. Krikunova, R. Kalms, F. Budzyn, O. Grimm, J. Rossbach, E. Ploenjes, M. Drescher, Nat. Photonics **3**, 523 (2009)
151. I. Grguraš, A.R. Maier, C. Behrens, T. Mazza, T.J. Kelly, P. Radcliffe, S. Düsterer, A.K. Kazansky, N.M. Kabachnik, T. Tschentscher, J.T. Costello, M. Meyer, M.C. Hoffmann, H. Schlarb, A.L. Cavalieri, Nat. Photonics **6**, 852 (2012)
152. W. Helml, A.R. Maier, W. Schweinberger, I. Grguraš, P. Radcliffe, G. Doumy, C. Roedig, J. Gagnon, M. Messerschmidt, S. Schorb, C. Bostedt, F. Grüner, L.F. DiMauro, D. Cubaynes,

J.D. Bozek, T. Tschentscher, J.T. Costello, M. Meyer, R. Coffee, S. Düsterer, A.L. Cavalieri, R. Kienberger, Nat. Photonics **8**, 950 (2014)

153. J.P. Cryan, J.M. Glownia, J. Andreasson, A. Belkacem, N. Berrah, C.I. Blaga, C. Bostedt, J. Bozek, C. Buth, L.F. DiMauro, L. Fang, O. Gessner, M. Guehr, J. Hajdu, M.P. Hertlein, M. Hoener, O. Kornilov, J.P. Marangos, A.M. March, B.K. McFarland, H. Merdji, V.S. Petrovic, C. Raman, D. Ray, D. Reis, F. Tarantelli, M. Trigo, J.L. White, W. White, L. Young, P.H. Bucksbaum, R.N. Coffee, Phys. Rev. Lett. **105**, 083004 (2010)

154. L. Young, E.P. Kanter, B. Kraessig, Y. Li, A.M. March, S.T. Pratt, R. Santra, S.H. Southworth, N. Rohringer, L.F. DiMauro, G. Doumy, C.A. Roedig, N. Berrah, L. Fang, M. Hoener, P.H. Bucksbaum, J.P. Cryan, S. Ghimire, J.M. Glownia, D.A. Reis, J.D. Bozek, C. Bostedt, M. Messerschmidt, Nature **466**, 56 (2010)

155. M. Hoener, L. Fang, O. Kornilov, O. Gessner, S.T. Pratt, M. Gühr, E.P. Kanter, C. Blaga, C. Bostedt, J.D. Bozek, P.H. Bucksbaum, C. Buth, M. Chen, R. Coffee, J. Cryan, L.F. DiMauro, M. Glownia, E. Hosler, E. Kukk, S.R. Leone, B. McFarland, M. Messerschmidt, B. Murphy, V. Petrovic, D. Rolles, N. Berrah, Phys. Rev. Lett. **104**, 253002 (2010)

156. L. Fang, M. Hoener, O. Gessner, F. Tarantelli, S.T. Pratt, O. Kornilov, C. Buth, M. Gühr, E.P. Kanter, C. Bostedt, J.D. Bozek, P.H. Bucksbaum, M. Chen, R. Coffee, J. Cryan, M. Glownia, E. Kukk, S.R. Leone, N. Berrah, Phys. Rev. Lett. **105**, 083005 (2010)

157. V.S. Petrovic, M. Siano, J.L. White, N. Berrah, C. Bostedt, J.D. Bozek, D. Broege, M. Chalfin, R.N. Coffee, J. Cryan, L. Fang, J.P. Farrell, L.J. Frasinski, J.M. Glownia, M. Gühr, M. Hoener, D.M.P. Holland, J. Kim, J.P. Marangos, T. Martinez, B.K. McFarland, R.S. Minns, S. Miyabe, S. Schorb, R.J. Sension, L.S. Spector, R. Squibb, H. Tao, J.G. Underwood, P.H. Bucksbaum, Phys. Rev. Lett. **108**, 253006 (2012)

158. B.K. McFarland, J.P. Farrell, N. Berrah, C. Bostedt, J. Bozek, P.H. Bucksbaum, R. Coffee, J. Cryan, L. Fang, R. Feifel, K. Gaffney, J. Glownia, T. Martinez, M. Mucke, B. Murphy, S. Miyabe, A. Natan, T. Osipov, V. Petrovic, S. Schorb, T. Schultz, L. Spector, F. Tarantelli, I. Tenney, S. Wang, W. White, J. White, M. Gühr, EPJ Web Conf. **41**, 07004 (2013)

159. J.D. Bozek, Eur. Phys. J.-Spec. Top. **169**, 129 (2009)

160. B.K. McFarland, N. Berrah, C. Bostedt, J. Bozek, P.H. Bucksbaum, J.C. Castagna, R.N. Coffee, J.P. Cryan, L. Fang, J.P. Farrell, R. Feifel, K.J. Gaffney, J.M. Glownia, T.J. Martinez, S. Miyabe, M. Mucke, B. Murphy, A. Natan, T. Osipov, V.S. Petrovic, S. Schorb, T. Schultz, L.S. Spector, M. Swiggers, F. Tarantelli, I. Tenney, S. Wang, J.L. White, W. White, M. Gühr, J. Phys. Conf. Ser. **488**, 012015 (2014)

161. V. Zhaunerchyk, M. Mucke, P. Salén, P. vd Meulen, M. Kaminska, R.J. Squibb, L.J. Frasinski, M. Siano, J.H.D. Eland, P. Linusson, R.D. Thomas, M. Larsson, L. Foucar, J. Ullrich, K. Motomura, S. Mondal, K. Ueda, T. Osipov, L. Fang, B.F. Murphy, N. Berrah, C. Bostedt, J.D. Bozek, S. Schorb, M. Messerschmidt, J.M. Glownia, J.P. Cryan, R.N. Coffee, O. Takahashi, S. Wada, M.N. Piancastelli, R. Richter, K.C. Prince, R. Feifel, J. Phys. B At. Mol. Opt. Phys. **46**, 164034 (2013)

162. L.J. Frasinski, V. Zhaunerchyk, M. Mucke, R.J. Squibb, M. Siano, J.H.D. Eland, P. Linusson, P. v.d. Meulen, P. Salén, R.D. Thomas, M. Larsson, L. Foucar, J. Ullrich, K. Motomura, S. Mondal, K. Ueda, T. Osipov, L. Fang, B.F. Murphy, N. Berrah, C. Bostedt, J.D. Bozek, S. Schorb, M. Messerschmidt, J.M. Glownia, J.P. Cryan, R.N. Coffee, O. Takahashi, S. Wada, M.N. Piancastelli, R. Richter, K.C. Prince, R. Feifel, Phys. Rev. Lett. **111**, 073002 (2013)

163. P.M. Hare, C.E. Crespo-Hernández, B. Kohler, Proc. Natl. Acad. Sci. **104**, 435 (2007)

164. T. Gustavsson, Á. Bányász, E. Lazzarotto, D. Markovitsi, G. Scalmani, M.J. Frisch, V. Barone, R. Improta, J. Am. Chem. Soc. **128**, 607 (2006)

165. M. Altarelli, Nucl. Instrum. Methods Phys. Res. Sect. B Beam Interact. Mater. At. **269**, 2845 (2011)

166. I. Schweigert, S. Mukamel, Phys. Rev. Lett. **99**, 163001 (2007)

167. S. Mukamel, D. Abramavicius, L. Yang, W. Zhuang, I.V. Schweigert, D.V. Voronine, Acc. Chem. Res. **42**, 553 (2009)

168. J.D. Biggs, Y. Zhang, D. Healion, S. Mukamel, J. Chem. Phys. **136**, 174117 (2012)

169. J.D. Biggs, Y. Zhang, D. Healion, S. Mukamel, J. Chem. Phys. **138**, 144303 (2013)

170. N. Rohringer, D. Ryan, R.A. London, M. Purvis, F. Albert, J. Dunn, J.D. Bozek, C. Bostedt, A. Graf, R. Hill, S.P. Hau-Riege, J.J. Rocca, Nature **481**, 488 (2012)
171. C. Weninger, M. Purvis, D. Ryan, R. London, J. Bozek, C. Bostedt, A. Graf, G. Brown, J. Rocca, N. Rohringer, Phys. Rev. Lett. **111**, 233902 (2013)
172. B.D. Patterson, R. Abela, H.-H. Braun, U. Flechsig, R. Ganter, Y. Kim, E. Kirk, A. Oppelt, M. Pedrozzi, S. Reiche, L. Rivkin, T. Schmidt, B. Schmitt, V.N. Strocov, S. Tsujino, A.F. Wrulich, New J. Phys. **12**, 035012 (2010)
173. E.-S. Kim, M. Yoon, I.E.E.E. Trans, Nucl. Sci. **56**, 3597 (2009)